OPEN ACCESS

Original research

Recurrent RhoGAP gene fusion CLDN18-ARHGAP26 promotes RHOA activation and focal adhesion kinase and YAP-TEAD signalling in diffuse gastric cancer

Feifei Zhang,[1,2] Varun Sahu,[3,4] Ke Peng,[2,5] Yichen Wang,[2,6] Tianxia Li,[3] Pratyusha Bala,[2] Daulet Aitymbayev,[2] Pranshu Sahgal ,[2] Antje Schaefer,[7,8] Channing J Der,[8,9] Sandra Ryeom,[10] Sam Yoon,[10] Nilay Sethi ,[2] Adam J Bass,[3,11] Haisheng Zhang [1,2,12]

► Additional supplemental material is published online only. To view, please visit the journal online (https://doi.org/10.1136/gutjnl-2023-329686).

For numbered affiliations see end of article.

Correspondence to
Dr Haisheng Zhang, 1838 Guangzhou Blvd N, Baiyun, Guangzhou, Guangdong Province, China; eslite3000@gmail.com and Dr Adam J Bass, 1130 St Nicholas Avenue, New York, NY 10032, USA; ab5147@cumc.columbia.edu

FZ and VS contributed equally. AJB and HZ contributed equally.

Received 10 February 2023
Accepted 8 February 2024

To cite: Zhang F, Sahu V, Peng K, *et al*. *Gut* Epub ahead of print: [*please include* Day Month Year]. doi:10.1136/gutjnl-2023-329686

ABSTRACT

Objective Genomic studies of gastric cancer have identified highly recurrent genomic alterations impacting RHO signalling, especially in the diffuse gastric cancer (DGC) histological subtype. Among these alterations are interchromosomal translations leading to the fusion of the adhesion protein CLDN18 and RHO regulator ARHGAP26. It remains unclear how these fusion constructs impact the activity of the RHO pathway and what is their broader impact on gastric cancer development. Herein, we developed a model to allow us to study the function of this fusion protein in the pathogenesis of DGC and to identify potential therapeutic targets for DGC tumours with these alterations.

Design We built a transgenic mouse model with *LSL-CLDN18-ARHGAP26* fusion engineered into the *Col1A1* locus where its expression can be induced by Cre recombinase. Using organoids generated from this model, we evaluated its oncogenic activity and the biochemical effects of the fusion protein on the RHOA pathway and its downstream cell biological effects in the pathogenesis of DGC.

Results We demonstrated that induction of *CLDN18-ARHGAP26* expression in gastric organoids induced the formation of signet ring cells, characteristic features of DGC and was able to cooperatively transform gastric cells when combined with the loss of the tumour suppressor gene*Trp53. CLDN18-ARHGAP26* promotes the activation of RHOA and downstream effector signalling. Molecularly, the fusion promotes activation of the focal adhesion kinase (FAK) and induction of the YAP pathway. A combination of FAK and YAP/TEAD inhibition can significantly block tumour growth.

Conclusion These results indicate that the *CLDN18-ARHGAP26* fusion is a gain-of-function DGC oncogene that leads to activation of RHOA and activation of FAK and YAP signalling. These results argue for further evaluation of emerging FAK and YAP-TEAD inhibitors for these deadly cancers.

WHAT IS ALREADY KNOWN ON THIS TOPIC

⇒ Recurrent translocations leading CLDN18-ARHGAP26 fusion proteins have been specifically found in diffuse gastric cancer (DGC). However, it has been unclear what are the functional effects of CLDN18-ARHGAP26 fusion in the stomach epithelium and potential therapies.

WHAT THIS STUDY ADDS

⇒ We functionally demonstrated that the CLDN18-ARHGAP26 fusion acts as an oncogene to promote the function of DGC when combined with Trp53 loss. We also found that focal adhesion kinase (FAK) and YAP were conserved downstream targets in these fusion-driven DGC. Finally, we found that the dual inhibitors of FAK and YAP-TEAD had significant synergistic effects upon inhibiting tumour growth, providing evidence for the future treatment of patients with DGC who have this recurrent fusion gene.

HOW THIS STUDY MIGHT AFFECT RESEARCH, PRACTICE OR POLICY

⇒ DGC is a highly lethal variant of GC prone to early invasion, rapid metastasis, poor survival and relative insensitive to current therapy. Defining the fundamental mechanisms of this disease and new effective therapies is of clear urgency. This study reveals fundamental disease mechanisms in DGC and connects them to new candidate therapies that can be prioritised for clinical trials.

INTRODUCTION

Gastric cancer (GC) is the fourth leading cause of cancer death worldwide, responsible for over 700 000 deaths every year.[1] The survival rates of GC are dismal, and we lack effective molecularly targeted therapies for most patients. Histologically, GC is classically divided into two types, intestinal and diffuse according to the Lauren classification.[2] Diffuse GC (DGC) lacks cellular cohesion and has typical features of highly invasive and poorly differentiated cancer cells, including mucin-enriched 'signet-ring' cells (also called signet ring cell carcinoma).[3] Molecularly, a large analysis from The Cancer Genome Analysis placed most DGCs into a category termed genomically stable tumours,

named as they lacked hypermutation and marked chromosomal instability. Within DGC, the most salient genome aberration is the loss of the tumour suppressor *CDH1* (encoding the cellular adhesion protein E-cadherin).[4] In hereditary DGC, *CDH1* is hemizygously inactivated in the germline.[4 5] Given the characteristic discohesive growth, and rapid invasion seen in DGC, a salient role for modulation of cell adhesion in its pathogenesis could be seen to follow logically. Beyond *CDH1* mutation, genomic characterisation by our group and others[3 6–9] identified recurrent genomic alterations impacting RHO pathway signalling in DGC. A first class of alterations are recurrent missense mutations (15%) of the RHOA GTPase, with the greatest recurrence for the Y42C hotspot mutation. Indeed, our team recently reported a detailed characterisation of $RHOA^{Y42C}$, which we established to act as an oncogene via impairing GTP hydrolysis (RHOA inactivation) and promoting RHOA interaction with ROCK, with resulting in enhanced actin rearrangements and focal adhesion formation.[10] These studies also revealed the activation of focal adhesion kinase (FAK) and the YAP pathway with results demonstrating the therapeutic potential of small-molecule FAK inhibition.[10]

Beyond RHOA mutation, the other most common mode (another 15% non-overlapping) of RHO pathway genomic dysregulation in DGC is with recurrent fusion genes that typically link the cellular adhesion protein Claudin18 (CLDN18) with RHO regulator ARHGAP26. Fusion genes have been reported to be involved as drivers in cancer formation and progression with notable examples including the Philadelphia chromosome leading to BCR-ABL fusion in patients with chronic myeloid leukaemia.[11] Similarly, EML4-ALK in patients with non-small cell lung cancer serves as both diagnostic biomarker and therapeutic target.[12 13] In DGC, recurrent CLDN18-ARHGAP26 fusions occur mutually exclusive with both mutations of *CDH1* and *RHOA*, suggesting it could supplant the functions of those aberrations. The most common version of the fusion leads to *CLDN18* (exon 5) becoming fused to the RHO modulator *ARHGAP26* (exon 12).[7] In this fusion, nearly the entire CLDN18 is retained, lacking only the C-terminal 11 amino acids and is linked to the C-terminal half of ARHGAP26. The ARHGAP26 sequence retains the catalytic GTPase activating domain (GAP), but is missing the adjacent pleckstring homology (PH) domain (online supplemental figure S1A). The PH domain occurs in a wide range of proteins involved in intracellular signalling or as constituents of the cytoskeleton, and is commonly involved in recruiting proteins to different cytoplasmic submembranes.[14 15] Shu *et al* performed a systematic investigation in patients with Chinese GC and identified a prevalence of 25% *CLDN18-ARHGAP26/6* fusions in signet-ring cell carcinoma, with patients with CLDN18-ARHGAP26/6 fusion having worse survival outcomes and little benefit from chemotherapy.[16] Nakayama *et al* also found 22 cases of *CLDN18-ARHGAP* (15.1%) in a population of 146 patients with GC, seeing the fusions associated with aggressive disease, poor prognosis and GCs in young adults.[17] Functional studies of the fusion to date are largely limited to those by Yao *et al*, who identified these fusions in GC and demonstrated that ectopic expression promotes loss of epithelial integrity in MCF10A cells.[18] However, it has been unclear what is the functional role of *CLDN18-ARHGAP26* fusions in the gastric epithelium and how the fusion contributes to the pathogenesis of DGC.

In this study, we demonstrated that expression of the *CLDN18-ARHGAP26* fusion together with *Trp53* loss, induces signet ring cells and tumour growth in mice. Using detailed biochemistry, we found *CLDN18-ARHGAP26* expression promotes activation of RHOA and downstream RHOA-ROCK effector signalling, stimulating actin reorganisation and focal adhesion formation. Furthermore, we demonstrated that *CLDN18-ARHGAP26* with *Trp53* loss induced DGC through activation of FAK and YAP-TEAD and we demonstrated that FAK and YAP-TEAD inhibition significantly abrogated tumour growth in xenografts model. In summary, these observations support FAK and YAP-TEAD as potential therapeutic targets for GCs with *CLDN18-ARHGAP26* fusion.

RESULTS

The recurrent gene fusion of *CLDN18-ARHGAP26* together with *Trp53*-loss induces diffuse gastric cancer in vivo

To systematically determine the function of *CLDN18-ARHGAP26* in the epithelium of the stomach, we built a transgenic mouse model with cre-recombinase inducible expression by establishing an allele with an *LSL-CLDN18-ARHGAP26* fusion engineered into the *Col1A1* locus (figure 1A). The *Mist1*-CreERT2 allele was introduced to express tamoxifen-activated Cre in the *Mist1* cells, a marker of gastric chief cells also demonstrated to be expressed in isthmus stem cells.[19–21] Finally, the *R26*-mTmG 'Tomato-GFP' allele was introduced to mark Cre-recombined cells by conversion from tomato (red) to GFP (green) (figure 1A). By breeding the cohorts of different mice, we could inducibly express *CLDN18-ARHGAP26* in gastric epithelium with the tracing marker from tomato to GFP (figure 1A). We then evaluated the expression of *CLDN18-ARHGAP26* in mice after in vivo tamoxifen induction. But unexpectedly, resembling the results seen with in vivo expression of the $RHOA^{Y42C}$ mutant allele, we observed severe body weight loss and death due to peritonitis several days after tamoxifen induction (data not shown). This effect, presumed to be due to loss of gastric epithelial integrity, complicated our original plan for evaluating the autochthonous expression of *CLDN18-ARHGAP26* and potential tumour formation in the gastric epithelium of mice.

Given the difficulty of in vivo induction of the fusion gene, we pivoted to developing gastric organoids from these mice, analogous to our earlier published studies of the mutant RHOA allele, to evaluate the effects of CLDN18-ARHGAP26 activity. We therefore induced expression of the fusion in vitro with tamoxifen treatment. Following induction, we found dramatic morphological changes, cell–cell adhesion markers and induction of mesenchymal markers (figure 1B and C, online supplemental figure S1B,G,H) in organoids expressing CLDN18-ARHGAP26 while the *Mist1*Cre organoids without the inducible fusion retained spherical forms with hollow morphology. The abnormal morphology of the *CLDN18-ARHGAP26* organoids included central filling of the organoid lumen with cells (figure 1B and C), a phenotype associated with transformation and consistent with morphologies of patient-derived DGC organoids.[9 22] By deeper histology review, we identified cells resembling signet-ring cells, a typical feature of DGC, in *CLDN18-ARHGAP26* organoids (figure 1D). To further validate the presence of signet-ring cells, we performed Alcian blue staining to monitor mucin expression, a marker of mucin formation secreted by signet ring cells. We found mucin-containing cells enriched in the *CLDN18-ARHGAP26* organoids but not the *Mist1*Cre control organoids (figure 1E).

We then found that *CLDN18-ARHGAP26* expression in organoids significantly increased cell proliferation via cell titre glo and Ki67 staining (figure 1F and G). To determine if these organoids were transformed, we transplanted cells (1×10^6 cells) into the flanks injection of *NOD.Cg-Prkdc^{scid} Il2rg^{tm1Wjl}/SzJ*

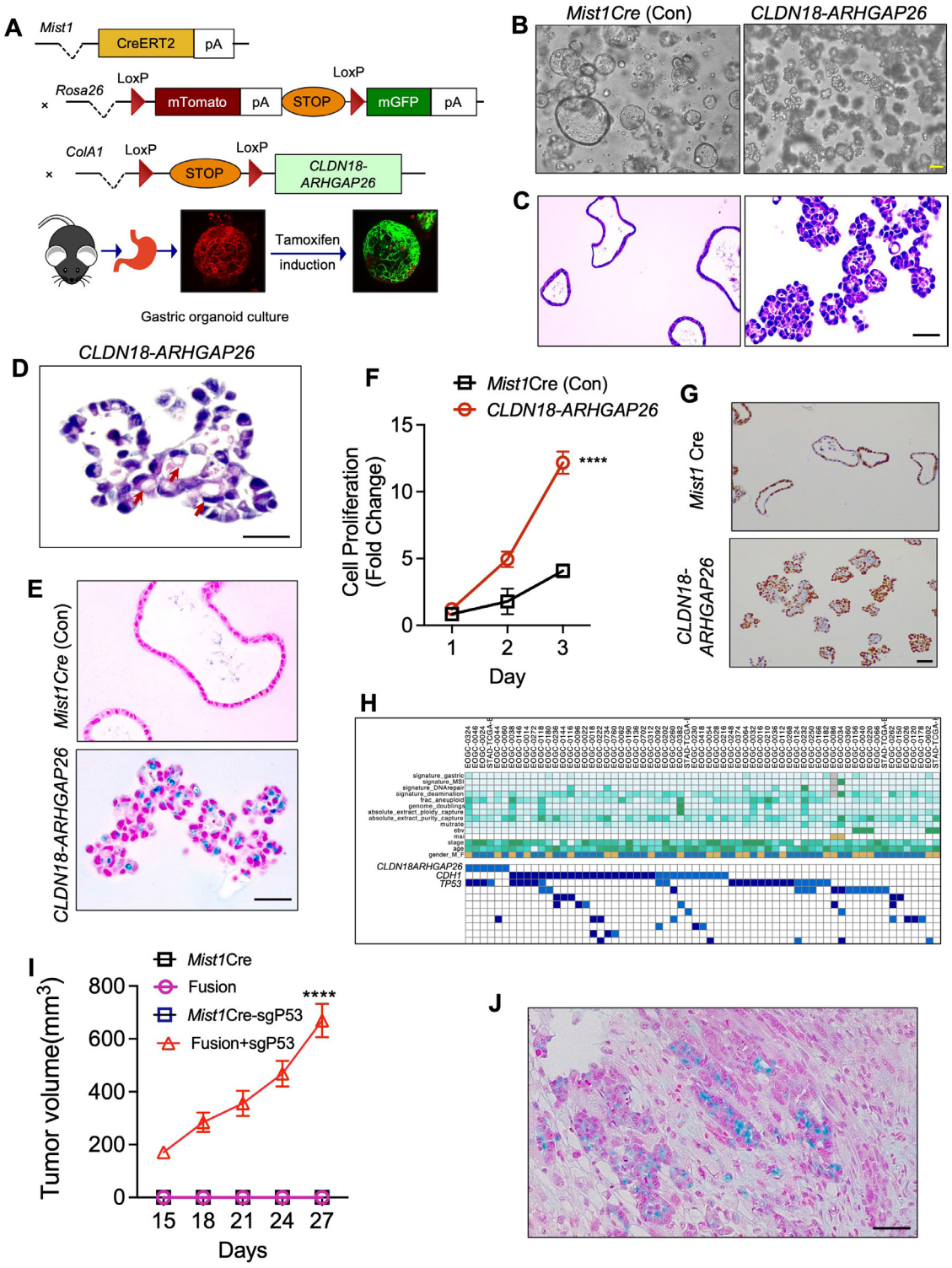

Figure 1 CLDN18-ARHGAP26 fusion induces abnormal organoid morphologies and signet ring cells. (A) Schematic for the generation of mice with distinct genotypes, including the tomato-GFP reporter allele; bottom: representative stack confocal image of gastric organoids with *Mist1*CreERT2-R26mTmG 48 hours after tamoxifen (2 µM) induction in vitro. Representative images of (B) phase contrast and (C) H&E for gastric organoids with annotated genotypes after 4 weeks following in vitro tamoxifen induction. Scale bar=100 µm. (D) Representative higher-magnification image showing signet ring cells in *CLDN18-ARHGAP26* fusion organoids following tamoxifen induction. Scale bar=50 µm. (E) Alcian blue staining of paraffin sections of the indicated organoids. Scale bar=100 µm. (F) In vitro proliferation (CellTiter-Glo) of *Mist1Cre* and *CLDN18-ARHGAP26* organoids. Data are mean±SD. ****p<0.0001, two-way ANOVA (*CLDN18-ARHGAP26* vs *Mist1*Cre). (G) Representative images of Ki67 staining of *Mist1Cre and CLDN18-ARHGAP* organoids. Scale bar=100 µm. (H) Analyses of co-occurrence of *Trp53* mutation and *CLDN18-ARHGAP* fusion. (I) Tumour volumes following NSG flank implantation of organoids with annotated genotypes, showing tumour formation only by *CLDN18-ARHGAP26* fusion organoids. Data are mean±SEM. ****p<0.0001, two-way ANOVA (*CLDN18-ARHGAP26* fusion with *P53* knockout vs other genotypes). (J) Representative image of Alcian blue staining for the *CLDN18-ARHGAP26* fusion with *Tp53* knockout tumours from panel (I). Scale bar=100 µm. ANOVA, analysis of variance; CLDN18, Claudin18.

(NSG) mice (figure 1I), finding that these *CLDN18-ARHGAP26* organoids were not able to form tumours alone. Suspecting that transformation may require additional cooperating lesions, we evaluated published genomic data, finding co-occurrence of *CLDN18-ARHGAP26* fusion with *Trp53* mutation (figure 1H), which was also described in other two other independent studies.[16 17] Therefore, we used CRISPR-Cas9 with sgRNA targeting *Trp53* to knockout p53 in the *CLDN18-ARHGAP26* fusion-expressing organoids. Implantation of these compound models revealed robust tumour growth. By contrast, no tumours formed with *Trp53 knockdown* or *Mist1*Cre control organoids (figure 1I). The histology results from the compound organoids demonstrated cells with signet ring morphology with additional undifferentiated cells, results consistent with the DGC phenotype (figure 1J). Next, we evaluated whether *Trp53* loss could affect the phenotype which we found in figure 1D–F. We found that *Trp53* loss coupled with *CLDN18-ARHGAP26* had similar phenotypes, including promoting cell proliferation and inducing abnormal morphology and signet ring cells compared with *Trp53* loss only, indicating that the tumour suppressor gene *Trp53* loss augmented the tumourigenic of *CLDN18-ARHGAP26* did not attenuate it's DGC histological features (online supplemental figure S1C-F).

CLDN18-ARHGAP26 promotes RHOA activity

As ARHGAP26 is an Rho GTPase activating protein, it promotes the transition from the active RHO-GTP form to the inactive RHO-GDP form, thus attenuating RHO signalling.[23] As the fusion links the bulk of the cellular adhesion protein CLDN18 with sequences encoded by exon 12 and above of *ARHGAP26*, the fusion may modulate the ARHGAP26 catalytic activity. We, therefore, evaluated how the *CLDN18-ARHGAP26* fusion expression impacts RHOA signalling in our murine gastric organoids. We first evaluated the interaction of RHOA with the isolated RHOA-GTP binding domain (RBD) of the RHOA effector Rhotekin (Rhotekin-RBD) to monitor formation of active RHOA-GTP. Despite ARHGAP26 acting as a GAP that promotes RHOA-GDP formation, we paradoxically found that CLDN18-ARHGAP26 enhanced rather than suppressed the level of RHOA-GTP (figure 2A). As active RHOA would enhance activity of downstream effector pathways, we confirmed ROCK effector activation by immunoblot analyses and found enhanced phosphorylation of Cofilin (pCofilin) in CLDN18-ARHGAP26 organoids compared with *Mist1*Cre organoids (figure 2B). Immunofluorescence microscopy studies revealed increased F-actin levels in *CLDN18-ARHGAP26* organoids compared with *Mist1*Cre organoids (figure 2C). These results were confirmed in parallel studies in the compound CLDN18-ARHGAP26 and *Trp53* models with similar results regarding RHOA pathway activation (online supplemental figure S2A,B). To further confirm our results, we established an isogenic organoid model from the gastric epithelia of mice with p53 knockdown and then introduced ectopic *CLDN18-ARHGAP26*. We found this ectopic induction of *CLDN18-ARHGAP26* also induced dramatic Rhotekin-RHOA binding and p-cofilin activation (figure 2D and E). We found that expression of the fusion gene (also in the context of p53 loss) enhanced active RHOA-GTP levels in the cell, as measured in effector Rhotekin pulldowns, and induced RHOA signalling, as determined by enhanced F-actin cytoskeleton and increased p-cofilin levels (figure 2F and G). Furthermore, To address whether the catalytic domain of ARHGAP26 is required for the function of CLDN18-ARHGAP26, we generated a new version of our fusion vector in which we introduced a missense mutation R293A, corresponding to R412A of ARHGAP26, which renders the fusion protein's Rho GAP catalytically inactive. We introduced this version of the fusion into our organoids and queried active-RhoA (Rhotekin) and the downstream p-Coffilin (online supplemental figure S2C,D). We found that R293A had little effect on the elevation of active-RHOA and downstream p-Coffilin by fusion. These data indicate that the GAP function is dispensable and suggest that the fusion might already lose the catalytic function of ARHGAP26, perhaps impairing the inhibitory activity on RHOA inhibition. These data support that the fusion gene may lose the RHO GTPase function and is a loss-of-function of ARHGAP26, leading to the activation of RHOA signalling. Overall, our studies show that CLDN18-ARHGAP26 causes a gain-of-function phenotype with RHOA activation and induction of RHOA downstream pathways.

CLDN18-ARHGAP26 induces activation of focal adhesion kinase

Having established that CLDN18-ARHGAP26 functions as an oncogene, we next evaluated the broader cellular and downstream effects of CLDN18-ARHGAP26 expression in the gastric lineage. As we described, CLDN18-ARHGAP26 is the fusion of CLDN18 and ARHGAP26, and ARHGAP26 is also known as GRAF (GTPase regulator associated with focal adhesion kinase).[24 25] Given both the described association of ARHGAP26 with FAK, our finding that CLDN18-ARHGAP26 increased the F-actin cytoskeleton which is associated with increased FAK activity, and our prior data linking oncogenic RHOA mutations to FAK, we next determined whether the fusion impacts FAK activity. We found that the P-FAK levels were elevated in the fusion-expressing organoids compared with *Mist1*-cre control organoids (figure 3A). We then determined whether FAK activity plays a functional role in the fusion organoids. We also evaluated the genetic targeting of the gene encoding FAK (*Ptk2*) in CLDN18-ARHGAP26 models. shRNA-mediated silencing of *Ptk2* phenocopied pharmacological inhibition of FAK and significantly inhibited the proliferation of CLDN18-ARHGAP26 fusion organoids (figure 3B). Furthermore, *Ptk2* loss also reverted the morphology of CLDN18-ARHGAP26 organoids, returning them to normal appearing hollow structures, (figure 3C) but had little effect on $Trp53^{-/-}Kras^{G12D/+}$ organoids, used as an alternative neoplastic control (online supplemental figure S3A–G).

We next determined that treatment with two chemically distinct pharmacological inhibitors of FAK, PF-573228 and defactinib, reversed the aberrant morphology caused by CLDN18-ARHGAP26 (figure 3D and E) in a dose-dependent manner (online supplemental figure S3B). In contrast, FAK inhibition had little effect on the morphology of $Trp53^{-/-}Kras^{G12D/+}$ organoids (online supplemental figure S3C). To further confirm our results, we performed Alcian blue staining and found the mucin-enriched cells were dramatically reduced by PF-573228 and defactinib treatment (figure 3F). FAK inhibitor treatment also inhibited the cell proliferation of organoids (figure 3G). We also determined the effect of FAK pertubations in the compound ARHGAP26 fusion and *Trp53* knockout model, and we found both the *PTK* genetic silencing and the drug treatments reversed the aberrant morphology and decreased the mucin staining (online supplemental figure S3D-F). PF-573228 and defactinib treatments also significantly inhibited cell proliferation of compound organoids (figure 3H).

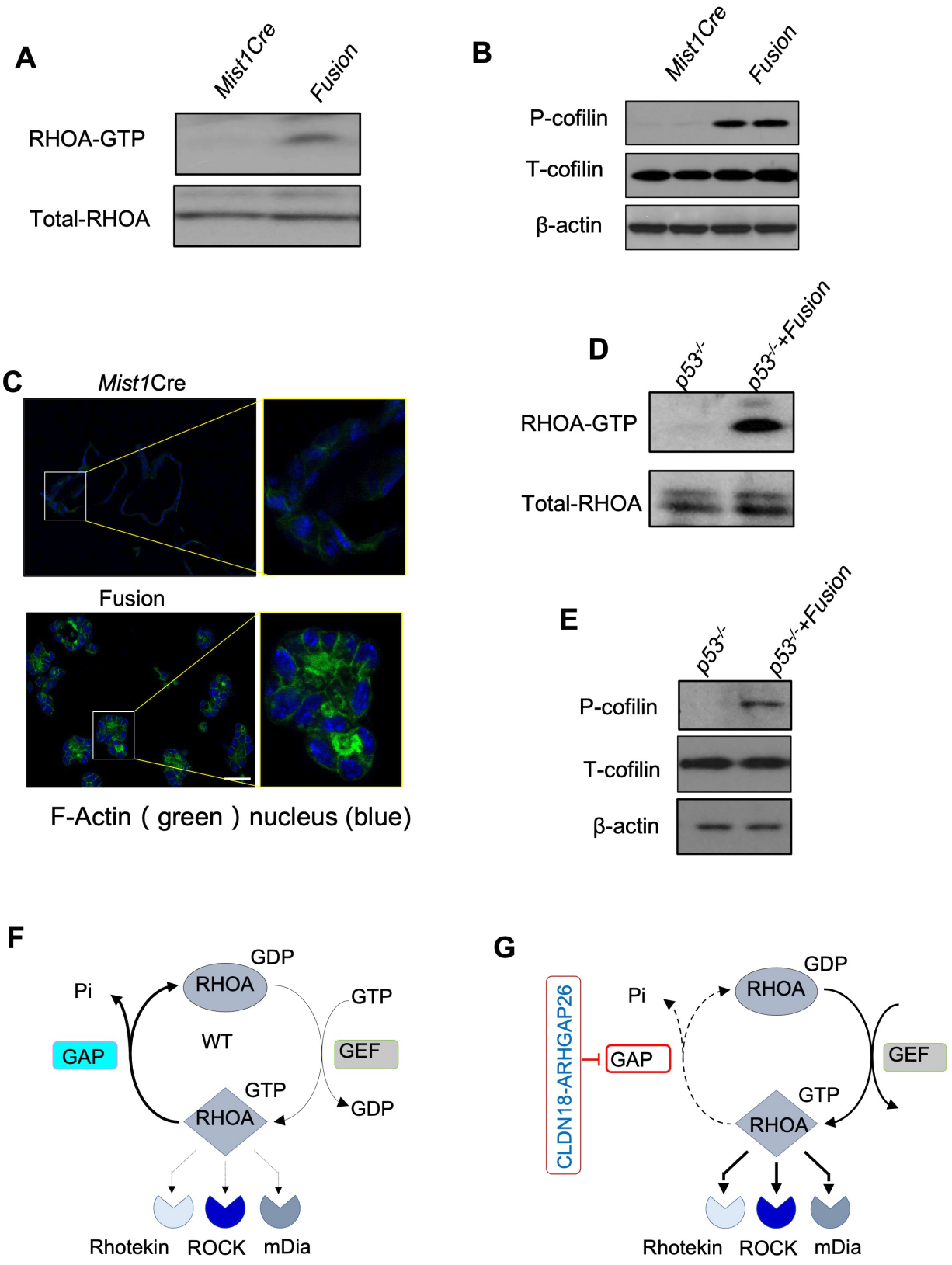

Figure 2 CLDN18-ARHGAP26 fusion promotes RHOA activity. (A) Immunoblotting for the RHOA binding of Rhotekin by Rhotekin pulldown assay. (Representative images from three independent experiments). (B) Immunoblotting for p-cofflin in the organoids with annotated genotype. Shown are representative images from three independent experiments. (C) Representative immunofluorescence images for F-actin in organoids from mice with annotated genotypes. Phalloidin (in green) was used to visualise F-actin, DAPI (in blue) for the nucleus. Scale bar=50 µm. (D) Immunoblotting for the Rhotekin-RBD pulldown assay with the *Tp53*$^{-/-}$ organoids engineered with lentiviral Control or *CLDN18-ARHGAP26* fusion. Shown are (representative images from three independent experiments). (E) Immunoblots of *P53*$^{-/-}$ organoids engineered with lentiviral vector or *CLDN18-ARHGAP26* plasmid (representative images from three independent experiments). Comparison of WT (F) and *CLDN18-ARHGAP26* fusion (G) biochemical properties. CLDN18, Claudin18; DAPI, 4′,6-diamidino-2-phenylindole; GAP, GTPase activating domain; WT, widetype.

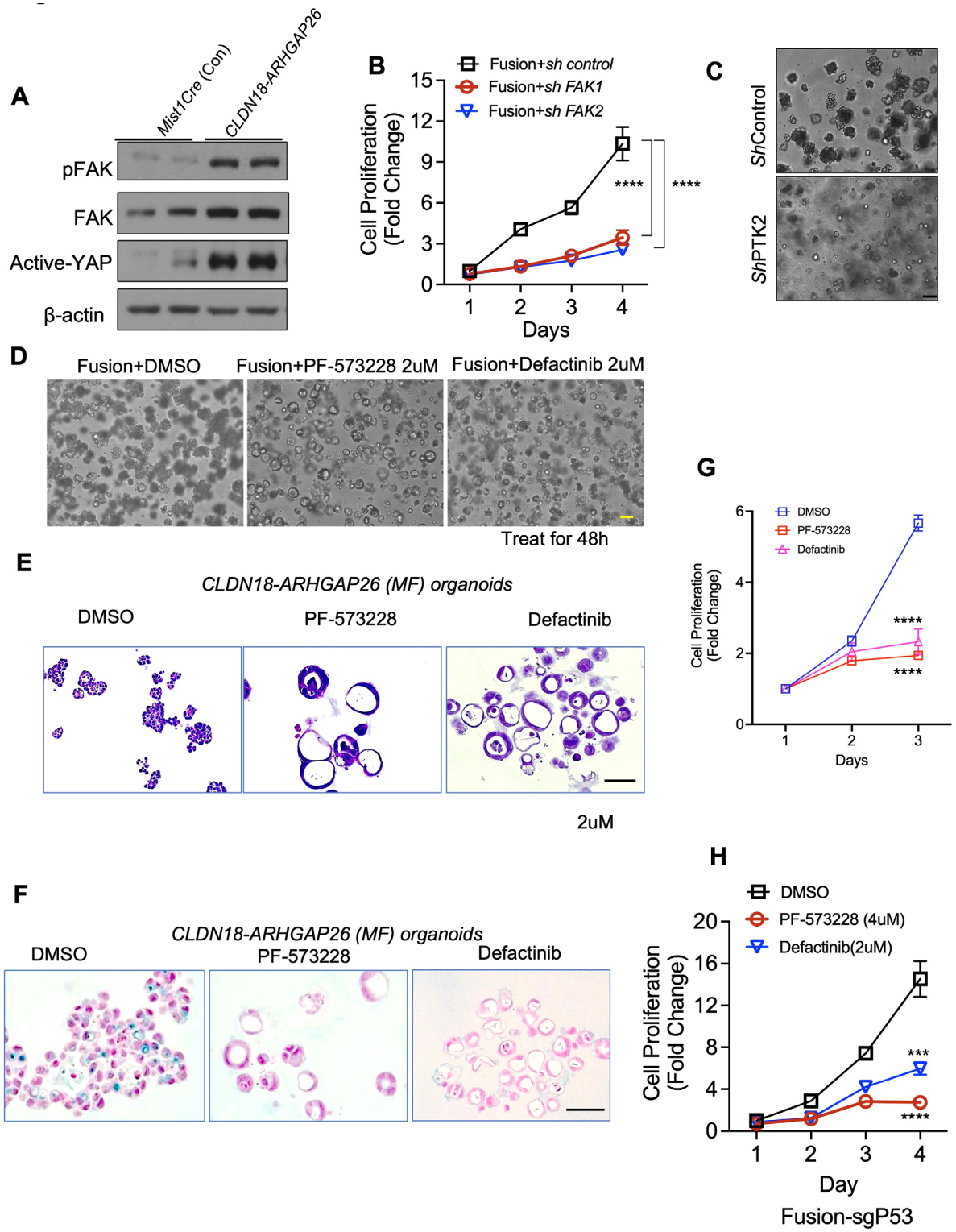

Figure 3 CLDN18-ARHGAP26 induces activation of focal adhesion kinase. (A) Immunoblotting for the organoids with annotated genotype. (Representative images from three independent experiments). (B) In vitro proliferation (CellTiter-Glo) of *CLDN18-ARHGAP26* organoids infected with control shRNA or targeting *Ptk2*. Data are mean± SD. ****p<0.0001, two-way ANOVA. (C) Representative images of phase contrast for gastric organoids with annotated genotypes scale bar=50 µm. Representative images of phase contrast (D) and H&E staining (E) for CLDN18-ARHGAP26 organoids treated with DMSO, PF-573228 (2 µM) or defactinib (2 µM) for 48 hours. Scale bar=100 µm. (F) Alcian blue staining of paraffin sections of the CLDN18-ARHGAP26 organoids treated with DMSO, PF-573228 (2 µM) or defactinib (2 µM) for 48 hours. Scale bar=100 µm. (G) In vitro proliferation (CellTiter-Glo) of *CLDN18-ARHGAP26* organoids treated with DMSO, PF-573228 (2 µM) or defactinib (2 µM). Data are mean±SD. ****p<0.0001, two-way ANOVA (PF-573228 or defactinib vs DMSO) (H) In vitro proliferation (CellTiter-Glo) of *CLDN18-ARHGAP26* with *Tp53* knockout organoids treated with DMSO or FAK inhibitors. Data are mean±SD. ***p<0.001, PF-573228 vs DMSO; ****p<0.0001, defactinib vs DMSO; two-way ANOVA. ANOVA, analysis of variance; CLDN18, Claudin18; DMSO, dimethyl sulfoxide; FAK, focal adhesion kinase; pFAK, phosphorylated focal adhesion kinase.

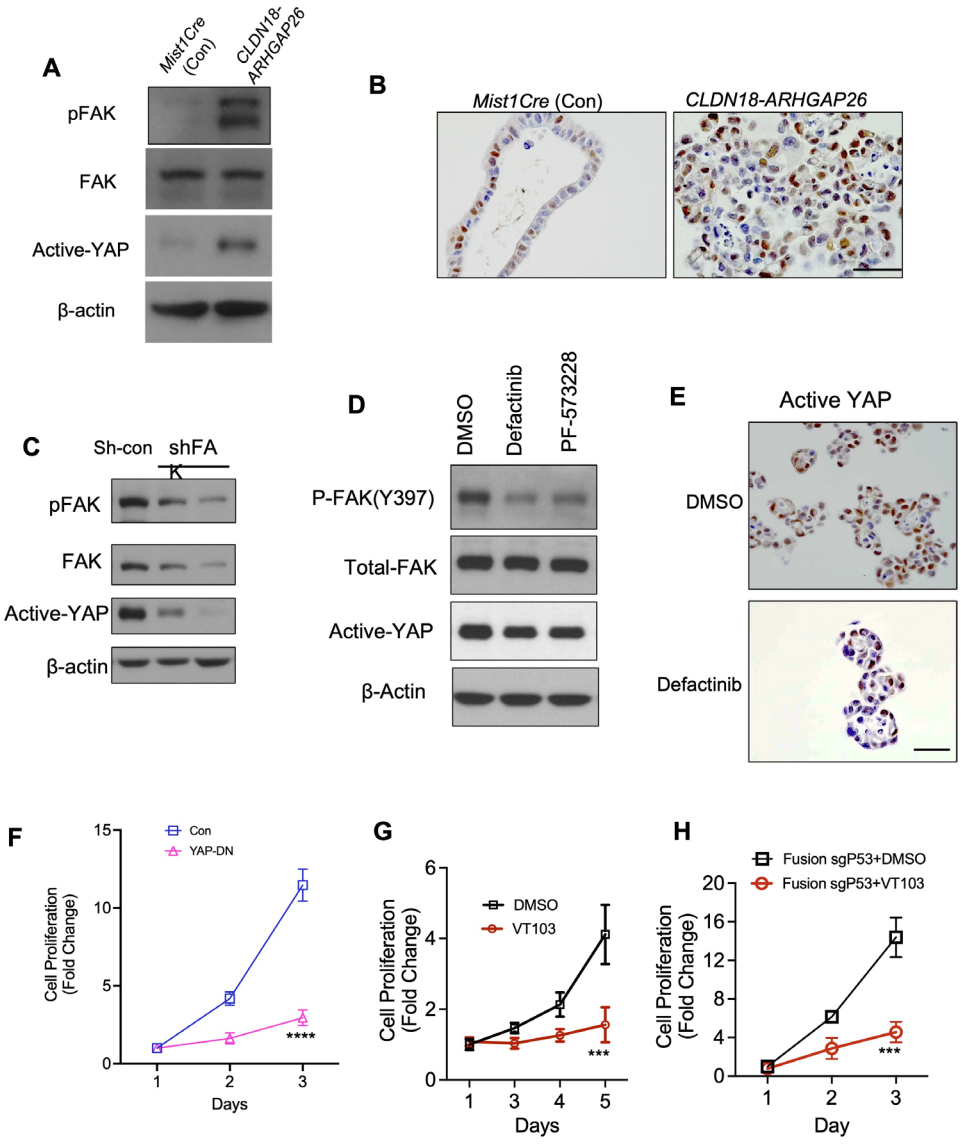

Figure 4 YAP is a potent downstream target of FAK in CLDN18-ARHGAP26. (A) Immunoblotting for the *Mist1*Cre organoids and the *CLDN18-ARHGAP26* organoids. (Representative images from three independent experiments). (B) Representative images of active-YAP staining for the organoids with annotated genotype. Scale bar=100 µm. (C) Immunoblotting for the *CLDN18-ARHGAP26* organoids engineered with *sh*Control or *shPTK2* virus (n=3 independent experiments). (D) Immunoblotting for the *CLDN18-ARHGAP26* organoids treated with DMSO, PF-573228 (2 µM) or defactinib (2 µM) for 48 hours (n=3 independent experiments). (E) Representative images of active-YAP staining for the paraffin sections of the CLDN18-ARHGAP26 organoids treated with DMSO or FAK inhibitor defactinib (2 µM). Scale bar=100 µm. (F) In vitro proliferation (CellTiter-Glo) of *CLDN18-ARHGAP26* organoids infected with control or YAP-DN expressing virus. Data are mean±SD. ****p<0.0001, two-way ANOVA (YAP-DN(S94A) vs DMSO). (G) In vitro proliferation (CellTiter-Glo) of *CLDN18-ARHGAP26* organoids treated with DMSO or TEAD inhibitor VT103 (2 µM). Data are mean±SD. ***p<0.0001, two-way ANOVA (VT103 vs DMSO). (H) In vitro proliferation (CellTiter-Glo) of *CLDN18-ARHGAP26* with p53 knockout organoids treated with DMSO or TEAD inhibitor VT103 (2 µM). Data are mean±SD. ***p<0.001, two-way ANOVA (VT103 vs DMSO). ANOVA, analysis of variance; CLDN18, Claudin18; DMSO, dimethyl sulfoxide; FAK, focal adhesion kinase; pFAK, phosphorylated focal adhesion kinase.

YAP is a potent downstream target of FAK in CLDN18-ARHGAP26

In our recent evaluation of the consequences of the RHOA^{Y42C} mutation in DGC, we found activation of the YAP pathway downstream of FAK signalling.[10] These findings are consistent with results in other recently published papers.[26 27] Therefore, we next evaluated if the fusion protein also promoted YAP activity. We found that active YAP levels were elevated in the CLDN18-ARHGAP26 organoids (figures 3A and 4A) and we found similar results in CLDN18-ARHGAP26/Trp53 null organoids (online supplemental figure S4A). Histological staining using an antibody against active-YAP also confirmed the results, with greater staining in the CLDN18-ARHGAP26 organoids compared with control organoids (figure 4B). We also found that both genetically and pharmacologically targeting FAK modulated active YAP levels in the context of fusion (figure 4C–E) and fusion with p53 loss (online supplemental figure S4B). This reduction in YAP activity was also observed when we looked at YAP target genes *CTGF, Cyr61, Myc and Ankrd1* (online supplemental figure S4H). To more comprehensively understand the function of other related signalling pathways, we performed blots for AKT/p-AKT, mTOR/p-mTOR and beta-catenin (online supplemental figure S4F,G) and found these pathways showed only slight changes.

Next, we asked whether YAP activation has a functional role in the fusion organoids. We first ectopically expressed the phospho-deficient YAP^{S94A} mutant (online supplemental figure S4C), that acts as a dominant-negative form of YAP, and found that YAP^{S94A} decreased cell proliferation in the CLDN18-ARHGAP26 fusion organoids (figure 4F, online supplemental figure S4D) but not in $Trp53^{-/-}Kras^{G12D/+}$ organoids (online supplemental figure S4E). We next evaluated whether pharmacologic inhibition of YAP, using VT103,[28] a small molecule inhibitor for the TEAD transcription factor, a key cofactor for YAP-driven gene expression. We found that TEAD inhibition impaired cell proliferation organoids expressing fusion alone, or in combination with *Trp53* null organoids (figure 4G and H). Overall, these data support YAP-TEAD signalling as a key downstream mediator of FAK activity in CLDN18-ARHGAP26 fusion organoids.

Dual inhibition of FAK and YAP/TEAD shows significant synergistic effects both in vitro and in vivo

We next evaluated the potential to combine treatment with FAK inhibition and YAP/TEAD. As the FAK inhibitor defactinib is now in the clinical trials, we chose to use this agent to combine with VT103. We first tested the combination in vitro in the CLDN18-ARHGAP26 fusion organoid model and we found the dual inhibition of FAK and TEAD markedly blocked the proliferation of fusion organoids relative to monotherapy with either agent (figure 5A). We also confirmed the efficacy of the combination results in the compound organoid model with the fusion together with the inactivation of tumour suppressor Trp53 gene and found similar results (figure 5B and online supplemental figure S5A). To further evaluate the combination of FAK and TEAD inhibitions, we evaluated these drugs alone and in combination therapies in vivo in NSG mice with flank implanted xenografts of fusion+Tp53 loss organoids. Individually, single agent defactinib (50 mg/kg) or VT103 (10 mg/kg) attenuated tumour growth. Tumour growth inhibition was again markedly increased with combination therapy as in the in vitro results (figure 5C). Further statistical testing of the in vivo growth data by two-way analysis of variance analysis showed there is a significant interaction between defactinib and VT103 treatment (figure 5C). Visual inspection of tumours confirmed the greater combination efficacy and we evaluated effects on phosphorylated FAK (pFAK) levels in vivo (figure 5D, online supplemental figure S5C,D). Encouragingly, there was little impact of the combination on body weight during therapy, consistent with tolerability of the regimen (online supplemental figure S5B).

Unfortunately, there are no available patient-derived models of DGC harbouring the CLDN18-ARHGAP26 fusion. However, we obtained two patient-derived organoid (PDO) models from patients with DGC. First, we evaluated the levels of active FAK and YAP in these two PDOs, using the Mist1Cre and fusion organoids as negative and positive controls, respectively. We found the two PDOs had comparable pFAK and an active YAP levels as the fusion murine model, suggesting the activity of these targets in the PDO models (figure 5E). We subsequently evaluated the combination of the two treatments in the two PDOs using a matrix of doses of the two drugs to allow us to calculate synergy scores, with this testing yielding results of a zero interaction potency (ZIP) score for PDO-DE66 was 21.1 (figure 5F) (ZIP score >10 being indicative of synergistic effect) and the synergy ZIP score for PDO-BL62 was 22.6 (figure 5G). Similarly, in combinations we saw enhanced inhibition of proliferation (figure 5H1) supporting the potential for YAP/TEAD and FAK inhibition in DGC.

DISCUSSION

Genomic studies of DGC have found highly frequent genomic alterations of CLDN18 -ARHGAP26 fusion,[7 16–18 23] a genomic event not known to occur in other classes of cancer. However, these genomic findings have yet to be translated into a deeper functional understanding of disease pathogenesis or into potential therapeutic targets. First, whether the formation of the *CLDN18-ARHGAP26* fusion protein drives activation or repression of RHO signalling had been uncertain. Yao *et al* reported that ectopic expression of CLDN18-ARHGAP26 inhibited RHOA-GTP levels and reduced and stress fibre formation in MCF10A breast epithelial cells in vitro.[18] The difference could be because of not only the different lineage but perhaps due to differences in organoid as compared with two-dimensional growth. Here we evaluated the effects of the fusion gene in stomach epithelial cells grown as organoids and found induction of RHOA, as measured by the increased of active GTP-bound RHOA in cells and induction of RHOA downstream signalling as determined by an enhanced p-cofilin levels and induction of the F-actin cytoskeleton. Moreover, the fusion demonstrated oncogenic activity, both in the induction of signet ring histological features in organoid growth and, when combined with p53 inactivation, with induction of tumour formation in vivo. These data indicated that the fusion could be a driver of DGC formation and progression as a similar function reported with other fusion genes (eg, *BCR-ABL*,[11] EML4-ALK[12]).

This report demonstrates fusion-induced activation of RHOA and its downstream signalling. Additional study will be required to define the detailed biochemical mechanisms by which this fusion impacts RHOA regulation. The fusion protein both removes the amino-terminal section of ARHGAP26, regions lacking the GAP domain and also tethers the GAP domain to the C-terminus of CLDN18, thus also impacting its intracellular localisation. Beyond the activity of the fusion in impacting RHO regulation another key cell biological question relates to its impact on cell adhesion given its inclusion of the tight junction protein CLDN18. Given the prominence of *CDH1*/E-cadherin loss in the pathogenesis of DGC and the exclusivity of CLDN18 fusions with *CDH1* loss, these results suggest that the fusion may dysregulate cell adhesion in a mode resembling the effects of the loss of the canonical *CDH1* tumour suppressor. Notably, the fusion retains nearly the full-length CLDN18 protein, but the attachment of the large C-terminal half of ARHGAP26 could impact CLDN18 interactions, resulting in broader effects on cell–cell interactions. Clinically, CLDN18 protein has been an attractive target due to CLDN18.2 targeting antibodies demonstrating efficiency in early-phase clinical trials such as the monoclonal antibody zolbetuximab[29] as well as emerging chimeric antigen receptor-T cell (CAR-T) therapies.[30] However, in the context of CLDN18-ARHGAP26 fusion protein, additional studies will be needed to identify the exact localisation of the fusion gene in the cell and the suitability of therapies that require cell surface expression of CLDN18 for efficacy.

With therapeutic relevance, we found that both FAK and YAP/TEAD were activated by *CLDN18-ARHGAP26* fusion, mirroring results from our earlier studies of the hotspot RHOA Y42C oncogene studied in concert with CDH1 inactivation in the gastric epithelium. Our pharmacologic and genetic inhibition of FAK suggests that FAK activity promotes YAP activation, paralleling data in other tissue types.[26 31 32] By itself, FAK inhibition can promote the normalisation of the morphology of the fusion organoids. However, we observed more robust antitumour effects both in vitro and in vivo via the combinatorial

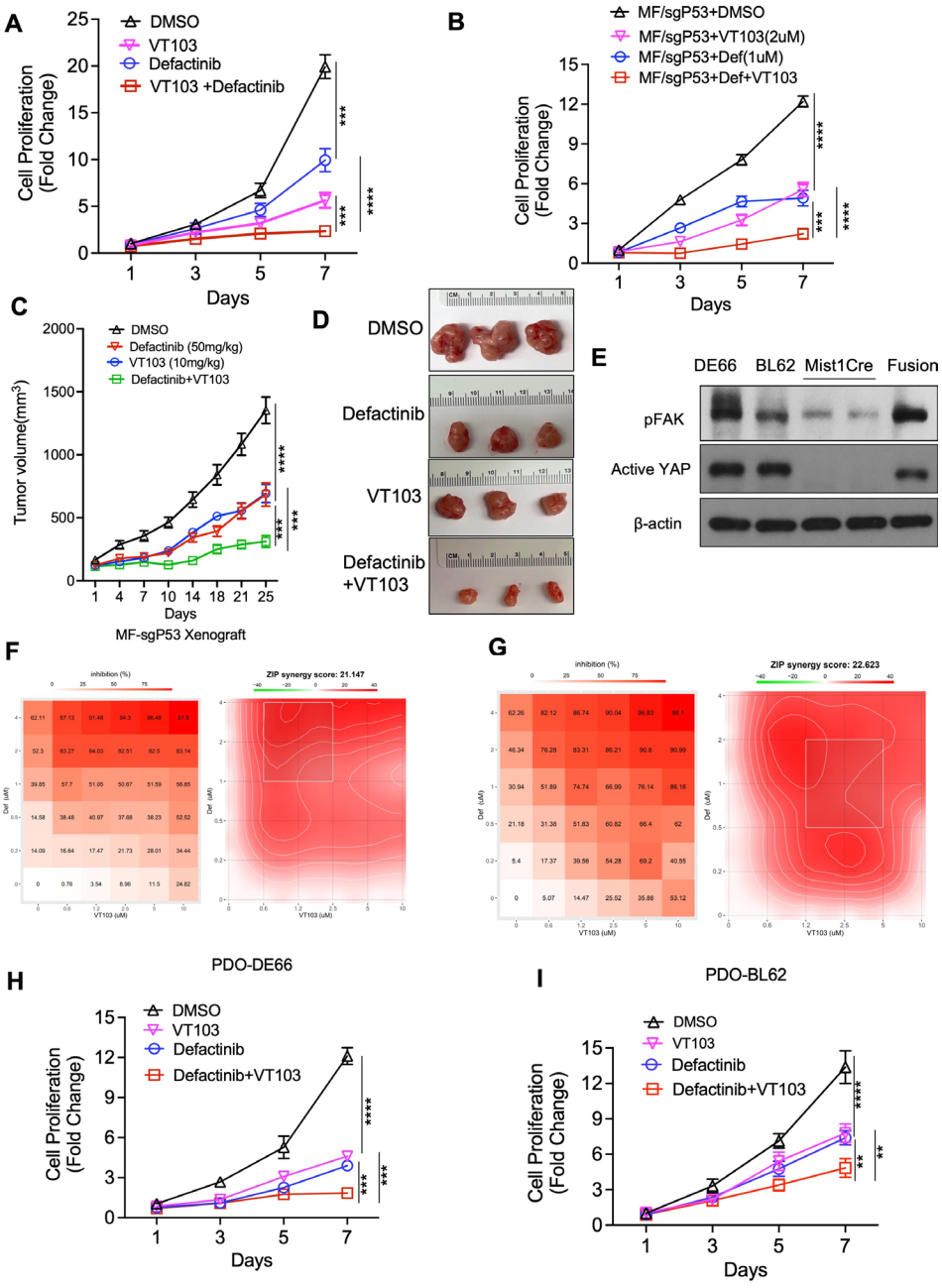

Figure 5 Dual inhibition of FAK and YAP/TEAD shows significant synergistic effects both in vitro and in vivo. (A) In vitro proliferation (CellTiter-Glo) of *CLDN18-ARHGAP26* with p53 knockout organoids treated with DMSO control, TEAD inhibitor VT103 (2 µM), defactinib (1 µM) or the combination. Data are mean±SD. ***p<0.001, ****p<0.0001, two-way ANOVA. (B) In vitro proliferation (CellTiter-Glo) of *CLDN18-ARHGAP26* with p53 knockout (MF/sgP53) organoids treated with DMSO control, TEAD inhibitor VT103 (2 µM), defactinib (1 µM) or the combination. Data are mean±SD. ***p<0.001, ****p<0.0001, two-way ANOVA. (C) Tumour growth curve for *CLDN18-ARHGAP26* with *Tp53* knockout organoids xenograft tumours (n=8–10) treated with vehicle control, defactinib (50 mg/kg, once a day), VT103 (10 mg/kg, once a day) or the combination. Day 1 means the first treatment of the drugs. Data are mean±SEM. ***p<0.001, ****p<0.0001, two-way ANOVA. (D) Representative tumour images of drug treatments from panel (C). (E) Representative immunoblotting images for the patient-derived organoids with the *Mist1*Cre (M) and *CLDN18-ARHGAP26* fusion (MF) organoids as controls (n=3 independent experiments). (F) DE66 patient-derived organoids (PDO-DE66) were treated with defactinib (0.2 µM to 4 µM) or VT103 (0.6 µM to 10 µM) alone or together for 7 days. Viability in the treatment groups was normalised to DMSO control. The inhibition rate was shown (left). Analysis of the synergistic effect in defactinib and VT103 combination was performed by SynergyFinder using zero interaction potency (ZIP) model. The inhibition rate was used to calculate ZIP synergy score. The box indicates the most synergistic area (right). Representatives of two independent experiments were shown. (G) BL62 patient-derived organoids (PDO-BL62) were treated with defactinib (0.2 µM to 4 µM) or VT103 (0.6 µM to 10 µM) alone or together for 5 days. Analysis of the synergistic effect in defactinib and VT103 combination was the same as in panel (F). In vitro proliferation (CellTiter-Glo) of PDO-DE66 (H) or PDO-BL62 (I) organoids were treated with DMSO, TEAD inhibitor VT103 (1 µM), defactinib (2 µM) or the combination. Data are mean± SD. **p<0.01, ***p<0.001, ****p<0.0001, two-way ANOVA. ANOVA, analysis of variance; CLDN18, Claudin18; DMSO, dimethyl sulfoxide; FAK, focal adhesion kinase; pFAK, phosphorylated focal adhesion kinase.

inhibition of FAK with emerging TEAD inhibitors which act via inhibition of palmitoylation of TEAD.[28] Furthermore, we found that the FAK and YAP were both activated in the DGC PDOs, and cell proliferation was inhibited by single agents or, more robustly, via combination treatments. In summary, these data provided a new foundation for mechanistic and translational inquiry into these deadly cancers and suggested a route to the development of rational targeted therapeutics using agents that are already in clinical testing.

METHODS

Generation of mouse cohorts

We generated a mouse allele with inducible expression of *CLDN18-ARHGAP26*. The human *RHOA* complementary DNA coding region with the Kozak sequence (GCCGCCACC) was introduced into vector pGV at the *EcoRI* cloning site using blunt-end cloning. Sequencing-confirmed pGV-CLDN18-ARHGAP26 vectors were co-electroporated with plasmid expressing FLP recombinase into mouse ES cells (MESC10, Mirimus) engineered with an FLP homing cassette at *Co1A1* locus, and positive clones were identified by PCR. Positive ES clones were injected into mouse blastocysts for chimaera generation. Chimeric mice were crossed with wildtype mice to generate mice with germline mutations. A detailed strategy was previously described.[33] The gene is expressed following Cre recombinase-mediated excision of a stop cassette flanked by *LoxP* sites (*loxP*-stop-*loxP* (LSL) *CLDN18-ARHGAP26*). *Mist1*-CreERT2, *R26*-mTmG mice were developed as previously published.[21] *Mist1*-CreERT2, *R26*-mTmG mice were crossed with LSL-*CLDN18-ARHGAP26* mice to generate *Mist1*-CreERT2, LSL-*CLDN18-ARHGAP26*, *R26*-mTmG mice. All animals were maintained and used in accordance with the guidelines of the Institutional Animal Care and Use Committee of the Dana-Farber Cancer Institute.

Organoids culture

CLDN18-ARHGAP26 mouse organoids were generated from *Mist1*-CreERT2, LSL-*CLDN18-ARHGAP26*, *R26*-mTmG mice above and cultured as previously described.[10] Two PDOs (PDO-DE66 and PDO-BL62) of human DGC were obtained from S. Ryeom (Columbia University) after having been generated from patients with GC under an institutional review board-approved protocol. All patients provided written informed consent, and the studies were conducted in accordance with the Declaration of Helsinki. For passaging, organoids were dissociated using TrypLE Express Enzyme (Gibco) at 37°C for 6 min. Cells (3×10^5) were mixed with 200 µL Matrigel (Corning, 354234) on ice. Six aliquots of the cell-Matrigel suspension (25–30 µL per aliquot) were seeded in a 6-well plate. To polymerise the Matrigel, plates were incubated at 37°C and upside down to avoid the attachment of cells to the plate surface. After 5 min, the plates were returned to the upright orientation. For mouse organoids, 2.5 mL 50% L-WRN conditioned medium[34] (a 1:1 mix of L-WRN conditioned medium and advanced Dulbecco's Modified Eagle Medium (DMEM)/F-12 with 20% fetal bovine serum (FBS)) were added. The medium for PDOs was described as previously.[35] CLDN18-ARHGAP26 mouse organoids organoids were passaged every 3 days. PDOs were passaged around 7 days based on growth dynamics. *Mycoplasma* tests were performed regularly using a Lonza MycoAlert Mycoplasma Detection Kit (Lonza, Basel, Switzerland).

Lentiviral infection of organoids

Lentiviral infection of organoids was performed as previously described. Briefly, cultured organoids were transferred in suspension (in 50% L-WRN conditioned media) into a 15 mL tube, centrifuged at 200×g for 5 min, resuspended in 200 µL trypsin-EDTA and incubated at 37°C for 5 min. Washing medium (1 mL) was added and the organoids were dissociated by vigorous pipetting. Organoids were centrifuged again at 200×g for 5 min and then the cells were resuspended in 250 µL solution containing lentivirus, 8 µg/mL polybrene and 10 µM Y27632 (R&D). Each suspension with a single lentivirus was then transferred to a single well of a 48-well plate, which was sealed with Parafilm (Bemis) and centrifuged at 600×g at 32°C for 1 hour. Plates were then incubated at 37°C for 6 hours to allow transduction. Cells were resuspended in conditioned organoid media (1 mL per well) and transferred to a 1.5 mL tube for centrifugation at 200×g for 5 min. Cells were resuspended in 20 µL Matrigel and cultured via our organoid culture method as listed above, except that the medium was supplemented with the appropriate antibiotics (eg, puromycin) for 7 days to deplete non-transduced organoid cells.

Subcutaneous xenograft tumours and drug treatment

For subcutaneous implantation. Cells were prepared from different genotypes of organoids and resuspended in 1:1 Matrigel:medium ratio. For each injection, 1×10^6 cells from in 200 µL mixture were injected subcutaneously into the flanks of NSG mice (6–8 weeks old) acquired from The Jackson Laboratory. Tumour volume was measured every 2 days via calliper measurement starting 2 weeks after injection. The tumour volume was calculated as $0.5\times a^2\times b$, where a is the width in millimetres and b is the length in millimetres. *For drug treatment*. Treatment was initiated when tumours reached approximately 100 mm^3. For FAK and TEAD inhibitor treatment, mice were randomised into four groups and intraperitoneally injected with vehicle dimethyl sulfoxide (DMSO) (0.5%) or defactinib (50 mg/kg) every day or with VT103 (10 mg/kg) every day for around 4 weeks. Mice treated with drug combinations received the same doses of each drug at the same intervals as the single-drug groups. All animal experiments were conducted in accordance with protocols approved by the Institutional Animal Care and Use Committee at the Dana-Farber Cancer Institute, in compliance with NIH guidelines.

Cell viability in organoid culture

A viability assessment was performed using the reagents and protocols from CellTiter-Glo (Promega G7570). On passage, 1000 cells were seeded in a single 5 µL Matrigel aliquot into each well of a 96-well plate containing 100 µL 50% L-WRN conditioned media. For drug treatments, inhibitors were added to the media at 24 hours after organoid plating. Organoids were cultured for the indicated days, then 50 µL of mixed CellTiter-Glo reagent was added to each well and the plate was gently shaken for 30 min at room temperature to allow the Matrigel to dissolve. Plates were read on a Tecan plate reader.

The synergy analyses were performed as previously[36] using the ZIP model.[37] Briefly, five different concentrations of each drug (0.25, 0.5, 1, 2 and 4 IC50) were administered, either alone or in combination. After the indicated number of days of treatment, cell viability was measured using the CellTiter-Glo assay. The results were analysed using SynergyFinder.[38]

Immunoblotting of organoids

After 3–5 days of growth, gastric organoids were collected and dissociated using TrypLE Express. Dissociated cells were plated

at a density of 40 000 cells per 25 µL Matrigel aliquot, with 7 Matrigel aliquots in 2.5 mL 50% L-WRN conditioned medium per well of a 6-well plate and allowed to grow for 24–36 hours before treatment with DMSO or the indicated drugs. Following drug treatment, the Matrigel surrounding the organoids was removed using Cell Recovery Solution (Corning). The released organoids were pelleted by centrifugation and lysed for immunoblotting as previously described.[36]

Antibodies and drugs

See online supplemental table S1.

Histology and immunohistochemistry staining

Tissues and organoids were processed for frozen sections or paraffin sectioning using protocols previously described.[10] For frozen sections, organoids were fixed in 4% paraformaldehyde in phosphate-buffered saline (PBS) at 4°C for 6 hours, then placed in 15% sucrose in PBS overnight, centrifuged and resuspended into bacto-agar and embedded in OCT (Tissue-Tek). The frozen sections were stained for F-actin using phalloidin. For paraffin sectioning, tissues were fixed in 10% formalin overnight and embedded in paraffin, whereas organoids were fixed in 10% formalin overnight, resuspended in bacto-agar, then embedded in paraffin. Standard protocols for sectioning paraffin-embedded tissues and staining with H&E or Alcian Blue staining were used. For Ki67 and active-YAP immunohistochemistry staining, slide deparaffinisation was followed by standard protocol. For the antigen retrieval: 250 mL of citric acid buffer was placed into a slide container, which was filled with up to 12 slides. The buffer solution was warmed in a microwave to 100°C for 10 min, then cooled for 5 min, warmed again for 2 min, cooled for 5 min, warmed again for 2 min, then cooled down to room temperature (RT). Citric acid was replaced with PBS, the slide container was placed onto a rocker and the slides were washed with PBS. The slides were then incubated in 10% H_2O_2 RT for 15 min followed by three washes in PBS. The slides were placed in a slide box and the tissue was circled using an oil pen. The tissue was incubated in bovine serum albumin (BSA) for 20 min, followed by incubation in the primary antibody overnight at 4°C. The slides were washed three times with PBS, incubated in secondary antibody (anti-rabbit serum, 1:200 in PBS) for 50 min, stained with DAB (3,3′-diaminobenzidine) (1:100), washed with H_2O, stained with haematoxylin and then mounted using standard protocol.

Rhotekin pulldown assay

The binding activity of RHOA to Rhotekin was performed by the Active Rho Pull-Down and Detection Kit (Thermo 16116). Collect the sample lysates from organoids as described above and save a sample of the cell lysate for protein assay using the Pierce BCA Protein Assay or 660 nm Protein Assay. Place a spin cup into a collection tube for each sample and swirl the bottle of Glutathione Resin to thoroughly resuspend the agarose beads. Add 100 µL of the 50% resin slurry to the spin cup with the collection tube and centrifuge the tubes at 6000×g for 10–30 s. Discard the flow-through and add 400 µL of Lysis/Binding/Wash Buffer to each tube with resin. Then invert the tubes gently several times. Centrifuge the tubes at 6000×g for 10–30 s and discard the flow-through. Thaw the GST-Rhotekin-RBD on ice and immediately make 400 µg aliquots. Add 400 µg of GST-Rhotekin-RBD to the spin cup containing the glutathione resin and immediately transfer up to 700 µL of the cell lysate (containing at least 500 µg of total proteins) to the spin cup, close the cap and vortex the sample. Seal cap of the collection tube with laboratory film to prevent leakage and vortex the sample. Incubate the reaction mixture at 4°C for 1 hour with gentle rocking. Centrifuge the spin cup with a collection tube at 6000×g for 10–30 s. Remove the laboratory film and transfer the spin cup to a new collection tube. Add 400 µL of Lysis/Binding/Wash Buffer, invert the tube three times and centrifuge at 6000×g for 10–30 s. Repeat this wash step two additional times. Transfer the spin cup to a new collection tube. Prepare 50 µL of reducing sample buffer for each pull-down reaction by mixing one part β-mercaptoethanol to 20 parts 2× SDS Sample Buffer and add 50 µL 2× reducing sample buffer to the resin. Vortex the sample and incubate at room temperature for 2 min. Centrifuge the tube at 6000×g for 2 min and remove and discard the spin cup containing the resin. Heat the eluted samples for 5 min at 95–100°C. Apply at least 25 µL per lane for a 10×10 cm mini-gel (12% acrylamide gel provides the best separation) and follow the western blot protocol.

Statistical analysis

Data are represented as mean±SD or SEM as indicated in the figure legends. For each experiment, the number of independent biological experiments are as noted in the figure legends, with representative images shown of replicates with similar results. Statistical analysis was performed using Prism V.7.0 (GraphPad). Pairwise comparisons between groups (ie, experimental vs control) were performed using an unpaired two-tailed Student's t-test or two-way analysis of variance as appropriate. P value<0.05 is considered to be statistically significant. P values are denoted by *p<0.05, **p<0.01, **p<0.001, ****p<0.0001. For all experiments, the variance between comparison groups was found to be equivalent. Sample sizes and animal numbers were determined from pilot laboratory experiments and previously published literature. Animals were excluded from analysis if they were euthanised due to health reasons unrelated to tumour growth. For in vivo experiments, all mice were randomised before drug treatment.

Author affiliations
[1]Department of General Surgery, Nanfang Hospital, Southern Medical University, Guangzhou, China
[2]Department of Medical Oncology, Dana-Farber Cancer Institute, Boston, Massachusetts, USA
[3]Department of Medicine, Columbia University Irving Medical Center, New York, New York, USA
[4]Department of Genetics and Development, Columbia University Irving Medical Center, New York, New York, USA
[5]Department of Medical Oncology, Fudan University, Shanghai, China
[6]Department of Pathology, Fudan University Shanghai Cancer Center, Shanghai, China
[7]Universty of North Carolina at Chapel Hill, Chapel Hill, North Carolina, USA
[8]Department of Pharmacology, University of North Carolina at Chapel Hill, Chapel Hill, North Carolina, USA
[9]University of North Carolina at Chapel Hill, Chapel Hill, North Carolina, USA
[10]Department of Surgery, Columbia University Irving Medical Center, New York, New York, USA
[11]Columbia University Vagelos College of Physicians and Surgeons, New York, New York, USA
[12]Signet Therapeutics, Shenzhen, China

Acknowledgements We thank Kwok-Kin Wong for overseeing generation of the novel murine allele.

Contributors HZ, AJB, FZ and VS designed the study and experiments. AJB and HZ provided resources and critical input. Methodology: FZ, VS, HZ, KP conducted the biochemical and cell culture experiments, FZ, HZ and YW performed the organoid experiments and FZ conducted the in vivo experiments. Guarantors: HZ and AJB. Writing—original draft, HZ, FZ; writing—review and editing, AJB, HZ, AS and CJD.

Funding This work was supported by grants from the National Cancer Institute (NCI) (R01 CA223775 to AJB and CJD), The V Foundation (AJB), The DeGregorio Family Foundation (AJB) and the Department of Defense Congressional Directed Medical Research Program (HZ) and National Natural Science Foundation of China

(No.82203302 to HZ). HZ was supported by AACR/Debbie's Dream Foundation. Histology and confocal core services were supported by the Harvard Digestive Disease Center and NIH grant P30DK034854.

Competing interests AJB has received funding from Merck, Novartis, Bayer and Repare, is the advisor to Earli and HelixNano and is now employed by the Novartis Institutes of Biomedical Research. AJB and HZ are co-founders and equity holders in Signet Therapeutics. CJD is an advisory board member for Deciphera Pharmaceuticals, Mirati Therapeutics, Reactive Biosciences, Revolution Medicines and SHY Therapeutics; has received research funding support from Boragen, Deciphera Pharmaceuticals, Mirati Therapeutics, Revolution Medicines and SpringWorks Therapeutics; and has consulted for Day One Biotherapeutics, Eli Lilly, Jazz Therapeutics, Ribometrix, Sanofi and Turning Point Therapeutics. All other authors do not report conflicts.

Patient and public involvement Patients and/or the public were not involved in the design, or conduct, or reporting, or dissemination plans of this research.

Patient consent for publication Not applicable.

Ethics approval Not applicable.

Provenance and peer review Not commissioned; externally peer reviewed.

Data availability statement All data relevant to the study are included in the article or uploaded as supplementary information.

ORCID iDs
Pranshu Sahgal http://orcid.org/0000-0002-9857-3987
Nilay Sethi http://orcid.org/0000-0002-3748-7559
Haisheng Zhang http://orcid.org/0000-0001-5220-5524

REFERENCES

1 Sung H, Ferlay J, Siegel RL, *et al*. Global cancer statistics 2020: GLOBOCAN estimates of incidence and mortality worldwide for 36 cancers in 185 countries. *CA Cancer J Clin* 2021;71:209–49.
2 Lauren P. The two histological main types of gastric carcinoma: diffuse and so-called intestinal-type carcinoma. An attempt at a histo-clinical classification. *Acta Pathol Microbiol Scand* 1965;64:31–49.
3 Kakiuchi M, Nishizawa T, Ueda H, *et al*. Recurrent gain-of-function mutations of RHOA in diffuse-type gastric carcinoma. *Nat Genet* 2014;46:583–7.
4 Guilford P, Hopkins J, Harraway J, *et al*. E-cadherin germline mutations in familial gastric cancer. *Nature* 1998;392:402–5.
5 Richards FM, McKee SA, Rajpar MH, *et al*. Germline E-cadherin gene (CDH1) mutations predispose to familial gastric cancer and colorectal cancer. *Hum Mol Genet* 1999;8:607–10.
6 Wang K, Yuen ST, Xu J, *et al*. Whole-genome sequencing and comprehensive molecular profiling identify new driver mutations in gastric cancer. *Nat Genet* 2014;46:573–82.
7 Cancer Genome Atlas Research Network. Comprehensive molecular characterization of gastric adenocarcinoma. *Nature* 2014;513:202–9.
8 Mun D-G, Bhin J, Kim S, *et al*. Proteogenomic characterization of human early-onset gastric cancer. *Cancer Cell* 2019;35:111–24.
9 Yan HHN, Siu HC, Law S, *et al*. A comprehensive human gastric cancer organoid biobank captures tumor subtype heterogeneity and enables therapeutic screening. *Cell Stem Cell* 2018;23:882–97.
10 Zhang H, Schaefer A, Wang Y, *et al*. Gain-of-function RHOA mutations promote focal adhesion kinase activation and dependency in diffuse gastric cancer. *Cancer Discov* 2020;10:288–305.
11 Pane F, Intrieri M, Quintarelli C, *et al*. BCR/ABL genes and leukemic phenotype: from molecular mechanisms to clinical correlations. *Oncogene* 2002;21:8652–67.
12 Koivunen JP, Mermel C, Zejnullahu K, *et al*. EML4-ALK fusion gene and efficacy of an ALK kinase inhibitor in lung cancer. *Clin Cancer Res* 2008;14:4275–83.
13 Stransky N, Cerami E, Schalm S, *et al*. The landscape of kinase fusions in cancer. *Nat Commun* 2014;5:4846.
14 Haslam RJ, Koide HB, Hemmings BA. Pleckstrin domain homology. *Nature* 1993;363:309–10.
15 Ingley E, Hemmings BA. Pleckstrin homology (PH) domains in signal transduction. *J Cell Biochem* 1994;56:436–43.
16 Shu Y, Zhang W, Hou Q, *et al*. Prognostic significance of frequent CLDN18-ARHGAP26/6 fusion in gastric signet-ring cell cancer. *Nat Commun* 2018;9:2447.
17 Nakayama I, Shinozaki E, Sakata S, *et al*. Enrichment of CLDN18-ARHGAP fusion gene in gastric cancers in young adults. *Cancer Sci* 2019;110:1352–63.
18 Yao F, Kausalya JP, Sia YY, *et al*. Recurrent fusion genes in gastric cancer: CLDN18-ARHGAP26 induces loss of epithelial integrity. *Cell Rep* 2015;12:272–85.
19 Stange DE, Koo B-K, Huch M, *et al*. Differentiated troy(+) chief cells act as reserve stem cells to generate all lineages of the stomach epithelium. *Cell* 2013;155:357–68.
20 Nam KT, Lee H-J, Sousa JF, *et al*. Mature chief cells are cryptic progenitors for metaplasia in the stomach. *Gastroenterology* 2010;139:2028–37.
21 Hayakawa Y, Ariyama H, Stancikova J, *et al*. Mist1 expressing gastric stem cells maintain the normal and neoplastic gastric epithelium and are supported by a perivascular stem cell niche. *Cancer Cell* 2015;28:800–14.
22 Nanki K, Toshimitsu K, Takano A, *et al*. Divergent routes toward WNT and R-spondin niche independency during human gastric carcinogenesis. *Cell* 2018;174:856–69.
23 Zhang L, Zhou A, Zhu S, *et al*. The role of GTPase-activating protein ARHGAP26 in human cancers. *Mol Cell Biochem* 2022;477:319–26.
24 Hildebrand JD, Taylor JM, Parsons JT. An SH3 domain-containing GTPase-activating protein for Rho and Cdc42 associates with focal adhesion kinase. *Mol Cell Biol* 1996;16:3169–78.
25 Taylor JM, Macklem MM, Parsons JT. Cytoskeletal changes induced by GRAF, the Gtpase regulator associated with focal adhesion kinase, are mediated by Rho. *J Cell Sci* 1999;112 (Pt 2):231–42.
26 Dawson JC, Serrels A, Stupack DG, *et al*. Targeting FAK in anticancer combination therapies. *Nat Rev Cancer* 2021;21:313–24.
27 Cell adhesion signaling regulates cancer stem cell dormancy after chemotherapy. *Cancer Discov* 2022;12:F4–OF4.
28 Tang TT, Konradi AW, Feng Y, *et al*. Small molecule inhibitors of TEAD auto-palmitoylation selectively inhibit proliferation and tumor growth of NF2-deficient mesothelioma. *Mol Cancer Ther* 2021;20:986–98.
29 Shitara K, Lordick F, Bang Y-J, *et al*. Zolbetuximab plus mFOLFOX6 in patients with CLDN18.2-positive, HER2-negative, untreated, locally advanced unresectable or metastatic gastric or gastro-oesophageal junction adenocarcinoma (SPOTLIGHT): a multicentre, randomised, double-blind, phase 3 trial. *Lancet* 2023;401:1655–68.
30 Qi C, Gong J, Li J, *et al*. Claudin18.2-specific CAR T cells in gastrointestinal cancers: phase 1 trial interim results. *Nat Med* 2022;28:1189–98.
31 Hu J-H, Du W, Shelton SJ, *et al*. An FAK-YAP-mTOR signaling axis regulates stem cell-based tissue renewal in mice. *Cell Stem Cell* 2017;21:91–106.
32 Song X, Xu H, Wang P, *et al*. Focal adhesion kinase (FAK) promotes cholangiocarcinoma development and progression via YAP activation. *J Hepatol* 2021;75:888–99.
33 Akbay EA, Moslehi J, Christensen CL, *et al*. D-2-hydroxyglutarate produced by mutant IDH2 causes cardiomyopathy and neurodegeneration in mice. *Genes Dev* 2014;28:479–90.
34 Miyoshi H, Stappenbeck TS. In vitro expansion and genetic modification of gastrointestinal stem cells in spheroid culture. *Nat Protoc* 2013;8:2471–82.
35 Vlachogiannis G, Hedayat S, Vatsiou A, *et al*. Patient-derived organoids model treatment response of metastatic gastrointestinal cancers. *Science* 2018;359:920–6.
36 Peng K, Zhang F, Wang Y, *et al*. Development of combination strategies for focal adhesion kinase inhibition in diffuse gastric cancer. *Clin Cancer Res* 2023;29:197–208.
37 Yadav B, Wennerberg K, Aittokallio T, *et al*. Searching for drug synergy in complex dose-response landscapes using an interaction potency model. *Comput Struct Biotechnol J* 2015;13:504–13.
38 Ianevski A, Giri AK, Aittokallio T. Synergyfinder 2.0: visual analytics of multi-drug combination synergies. *Nucleic Acids Res* 2020;48:W488–93.

Figure S1

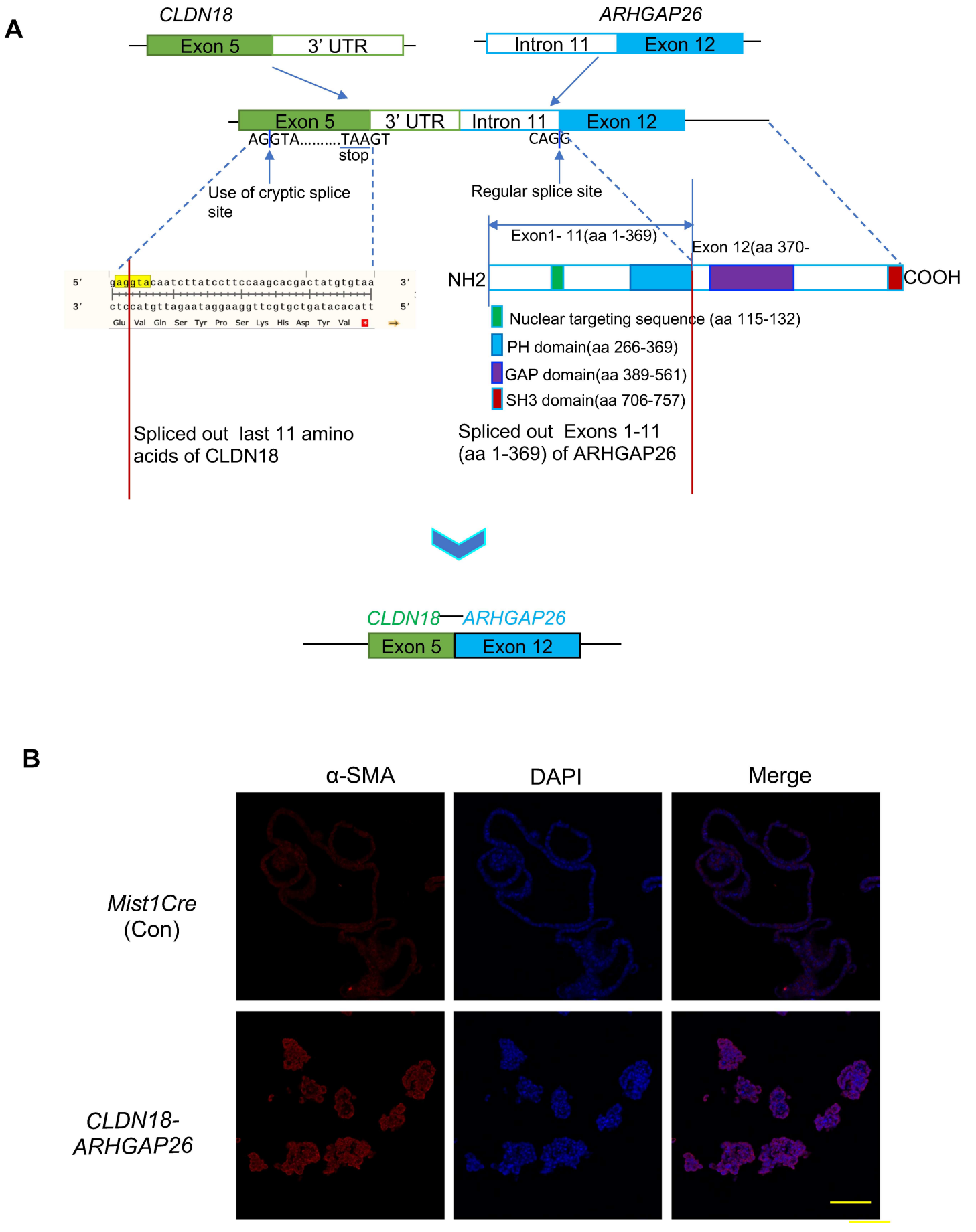
A
CLDN18
Exon 5
3' UTR
ARHGAP26
Intron 11
Exon 12
Exon 5
3' UTR
Intron 11
Exon 12
AGGTA.....TAAGT
stop
CAGG
Use of cryptic splice site
Regular splice site
Exon1- 11(aa 1-369)
Exon 12(aa 370-
NH2
COOH
Nuclear targeting sequence (aa 115-132)
PH domain(aa 266-369)
GAP domain(aa 389-561)
SH3 domain(aa 706-757)
Spliced out last 11 amino acids of CLDN18
Spliced out Exons 1-11 (aa 1-369) of ARHGAP26
CLDN18—ARHGAP26
Exon 5
Exon 12
B
α-SMA
DAPI
Merge
Mist1Cre (Con)
CLDN18-ARHGAP26

Figure S1

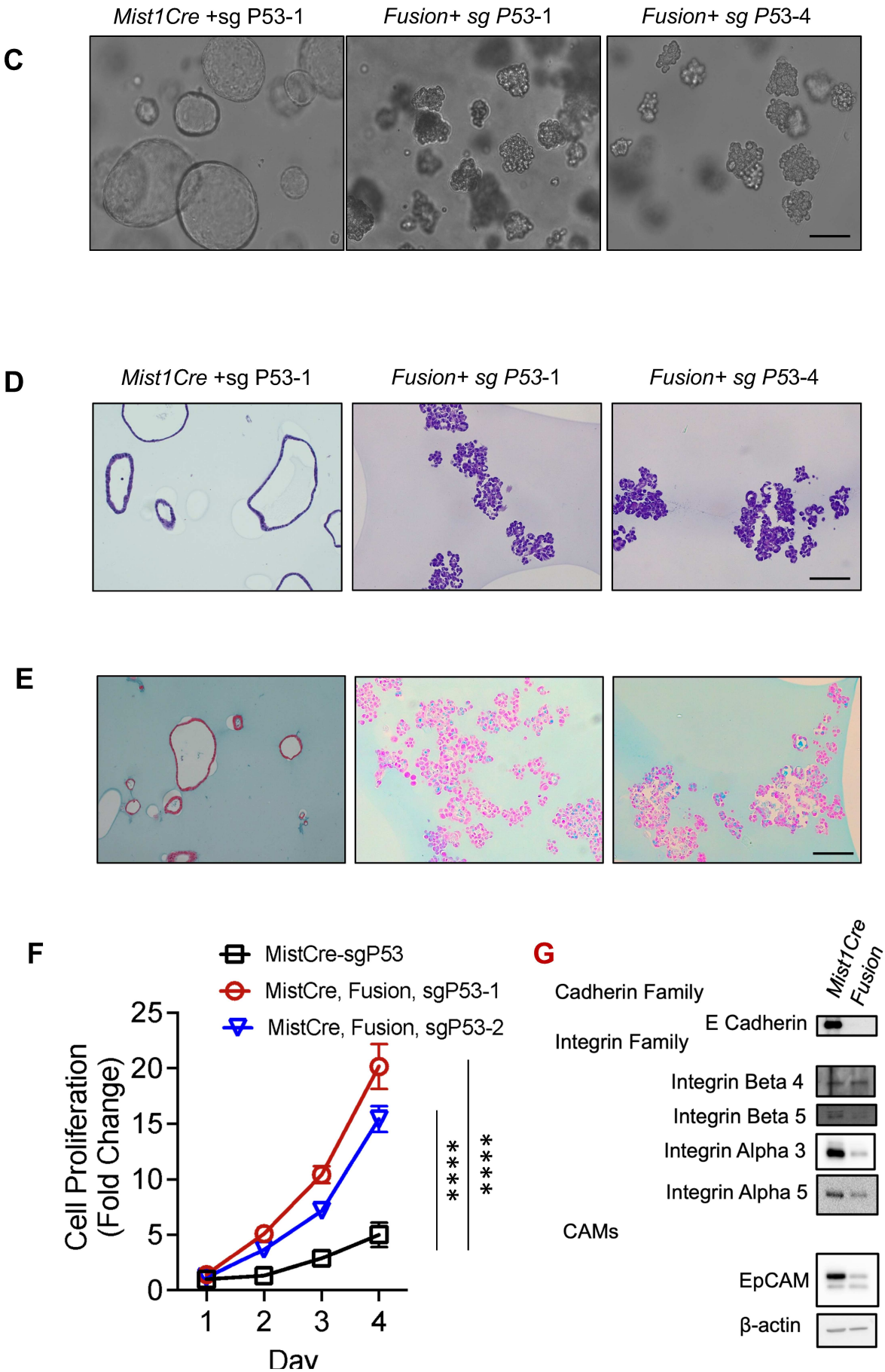
C
Mist1Cre +sg P53-1
Fusion+ sg P53-1
Fusion+ sg P53-4
D
Mist1Cre +sg P53-1
Fusion+ sg P53-1
Fusion+ sg P53-4
E
F
MistCre-sgP53
MistCre, Fusion, sgP53-1
MistCre, Fusion, sgP53-2
Cell Proliferation (Fold Change)
25
20
15
10
5
0
1
2
3
4
Day
****
****
G
Mist1Cre
Fusion
Cadherin Family
E Cadherin
Integrin Family
Integrin Beta 4
Integrin Beta 5
Integrin Alpha 3
Integrin Alpha 5
CAMs
EpCAM
β-actin

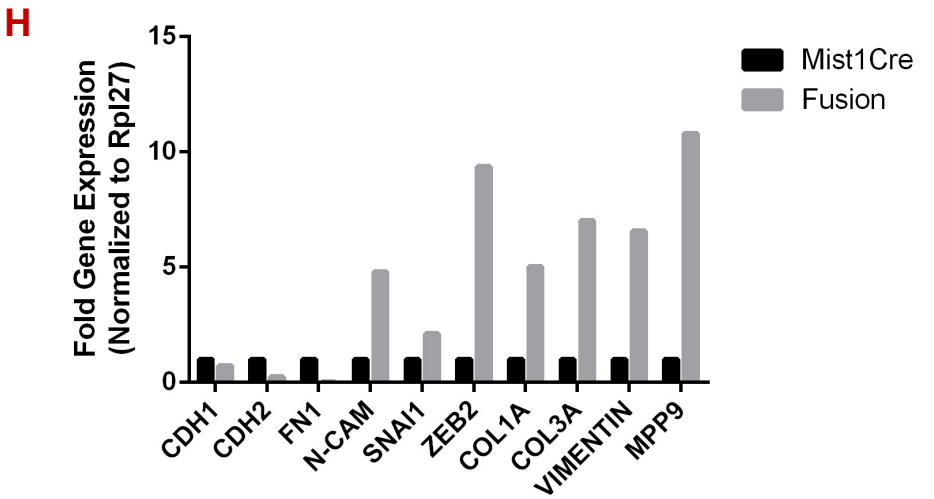

Supplementary Figure 1. CLDN18-ARHGAP26 fusion induces abnormal organoid morphologies and co-occurrence with P53 inactivation

A, Schematic of CLDN18 fused with ARHGAP26 for the fusion transcript and predicted fusion protein. PH domain: Pleckstrin homology domain; SH3: SRC homology 3 domain; GAP domain: GTPase activating domain. **B**, Confocal immunofluorescence images of α-SMA in the indicated organoids. Scale bar = 100 μm. (**C**) phase contrast and (**D**) H&E and (**E**) Alcian Blue for gastric organoids with annotated genotypes with P53 knockout. Scale bar = 100 μm. **F,** *In vitro* proliferation (CellTiter-Glo) of *Mist1Cre* and *CLDN18-ARHGAP26* organoids knockout with *Trp53*. Data are mean ± S.D. ****P<0.0001, two-way ANOVA. **G,** Immunoblotting of proteins involved in cell-to-cell adhesion and maintaining epithelial integrity in *Mist1Cre* and *CLDN18-ARHGAP26* fusion organoids (representative images from 3 independent experiments). **H,** Quantitative real time PCR for epithelial and mesenchymal genes in *Mist1Cre* and *CLDN18-ARHGAP26* organoids (n=3).

Figure S2

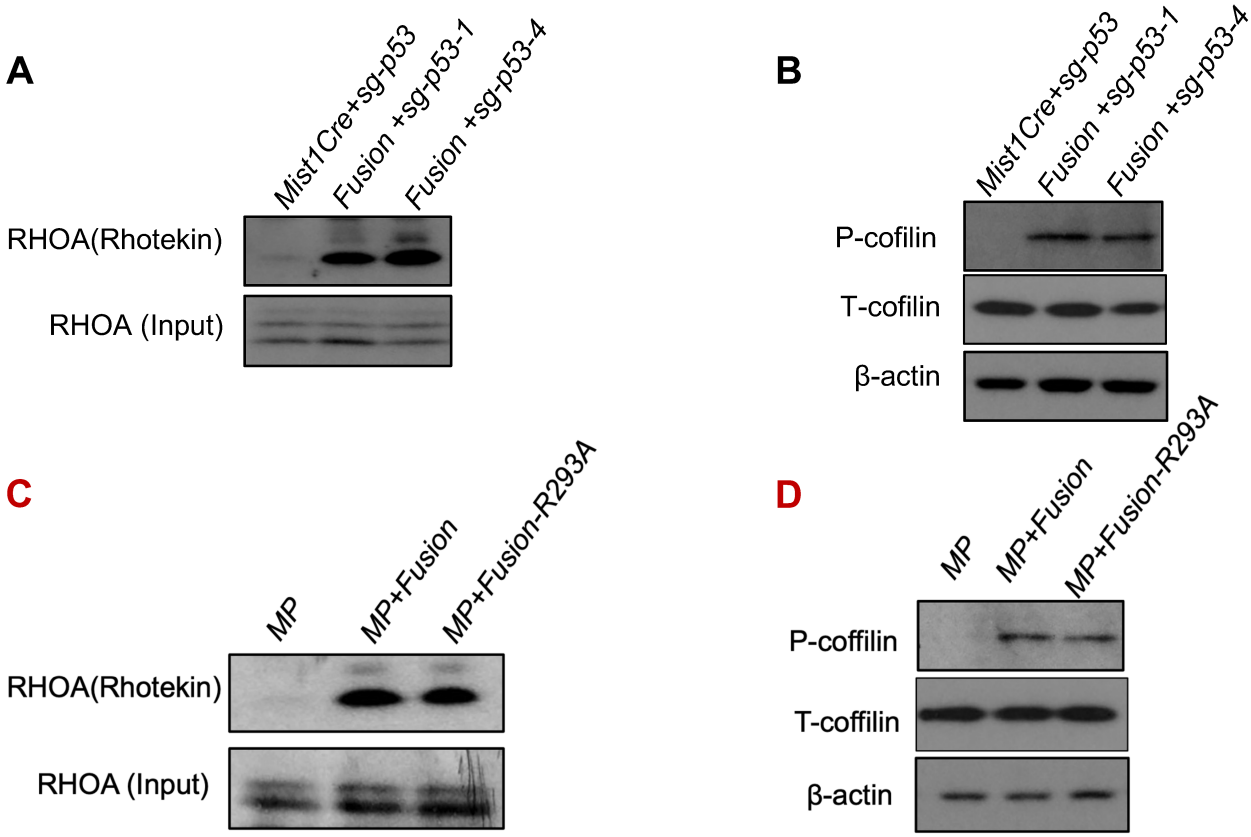

Supplementary Figure 2. CLDN18-ARHGAP26 fusion promotes the RHOA signaling activity.

A, Immunoblotting for the RHOA binding of Rhotekin by Rhotekin-pulldown assay with sg-p53. (representative images from 3 independent experiments). **B,** Immunoblotting for p-cofilin in the organoids with annotated genotype (representative images from 3 independent experiments). **C,** Immunoblotting for the RHOA binding of Rhotekin by Rhotekin-pulldown assay with fusion or fusion missense mutation of corresponding to R293A of ARHGAP26 (n= 3 independent experiments). **D**, Immunoblotting for p-cofilin and t-cofilin in the organoids with annotated genotype (representative images from 3 independent experiments).

Figure S3

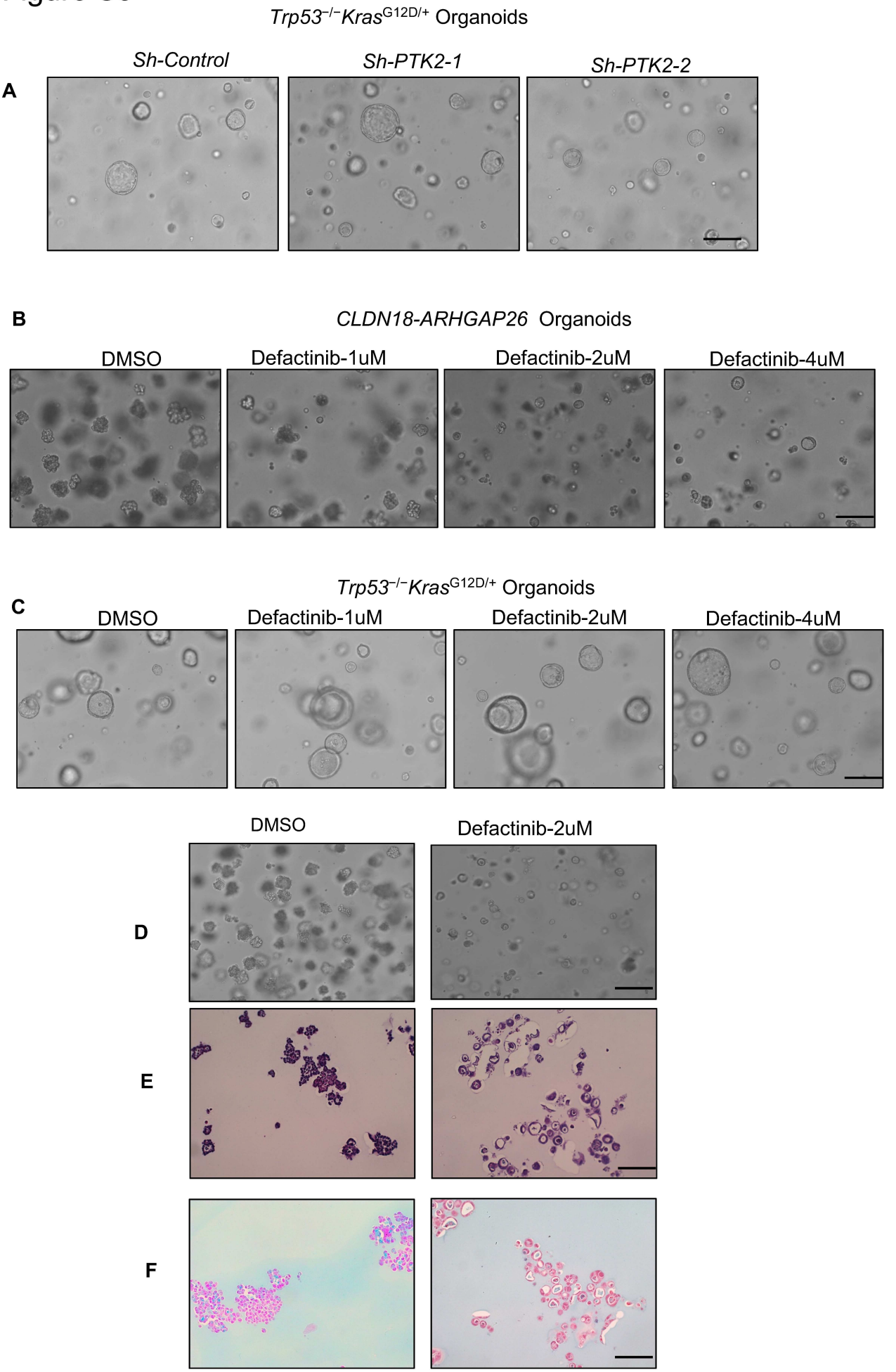
Trp53$^{-/-}$*Kras*$^{G12D/+}$ Organoids
A
Sh-Control
Sh-PTK2-1
Sh-PTK2-2
B
CLDN18-ARHGAP26 Organoids
DMSO
Defactinib-1uM
Defactinib-2uM
Defactinib-4uM
Trp53$^{-/-}$*Kras*$^{G12D/+}$ Organoids
C
DMSO
Defactinib-1uM
Defactinib-2uM
Defactinib-4uM
DMSO
Defactinib-2uM
D
E
F

G

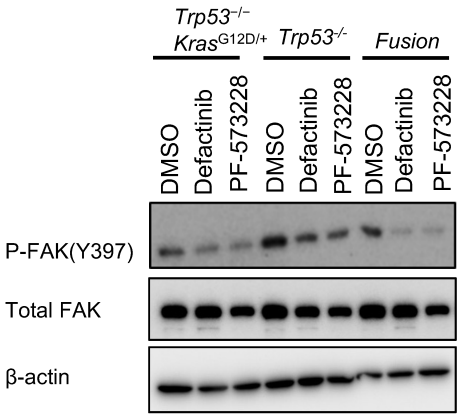

Supplementary Figure 3. FAK inhibition reversed the abnormal morphologies of CLDN18-ARHGAP26.

A, Phase contrast of *Trp53*$^{-/-}$*Kras*$^{G12D/+}$ Organoids knockdown with *sh*Control or *sh*FAK(PTK2). **B**, Representative images of phase contrast of CLDN18-ARHGAP26 organoids treated with DMSO and indicated dose of defactinib for 48h . **C**, Representative images of phase contrast of *Trp53*$^{-/-}$*Kras*$^{G12D/+}$ organoids treated with DMSO and indicated dose of defactinib for 48h . Representative images of (**D**) phase contrast and (**E**) H&E and (**F**) Alcian Blue for CLDN18-ARHGAP26 organoids t with *Trp53* knockout. Scale bar = 100 μm. **G,** Immunoblotting *Trp53*$^{-/-}$*Kras*$^{G12D/+}$, *Trp53*$^{-/-}$ and *CLDN18-ARHGAP26* fusion organoids upon treatment with DMSO, PF-573228 (2 μM) or Defactinib (2 μM) for 48h (representative images from 3 independent experiments).

Figure S4

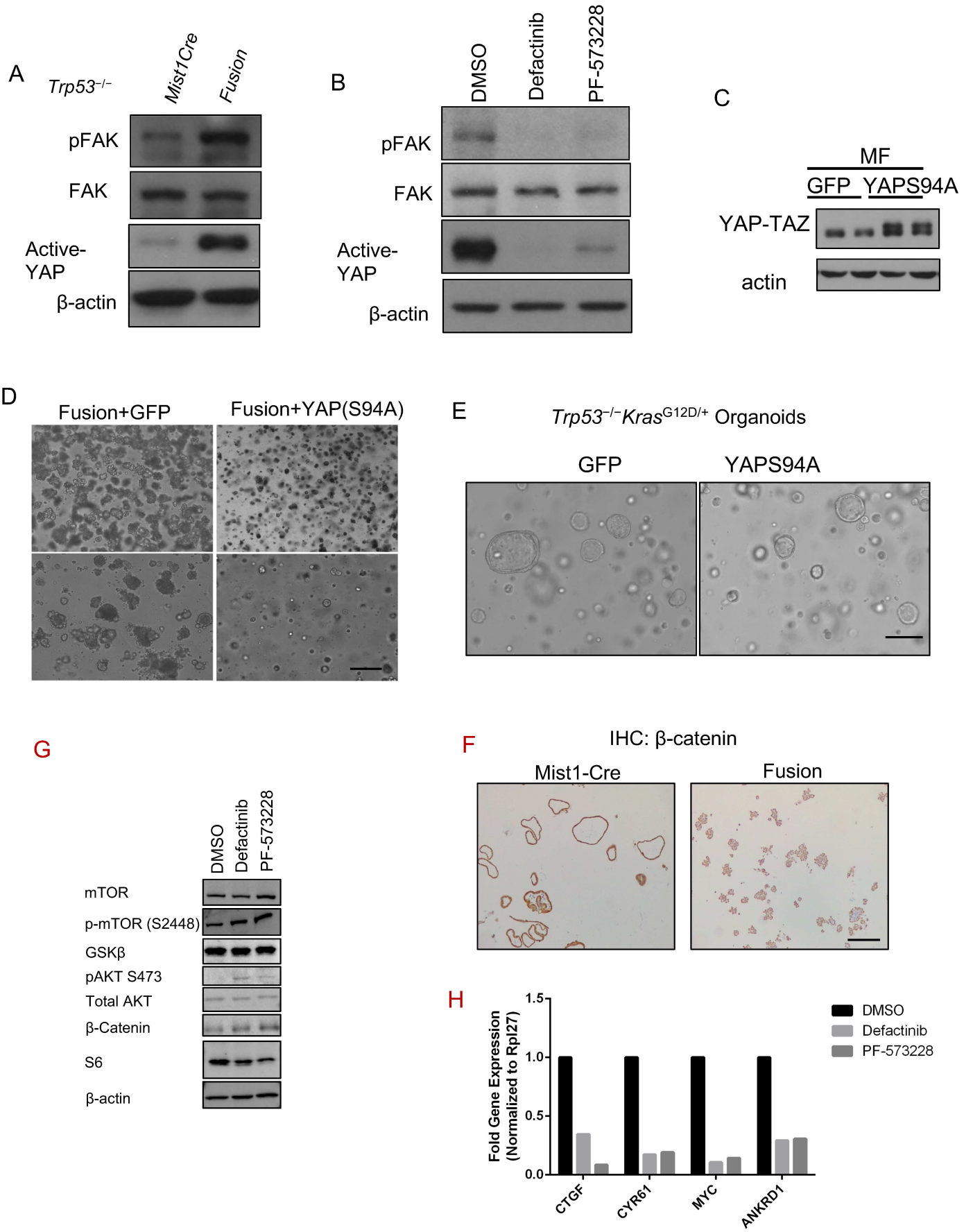
A
Trp53−/−
Mist1Cre
Fusion
pFAK
FAK
Active-YAP
β-actin
B
DMSO
Defactinib
PF-573228
pFAK
FAK
Active-YAP
β-actin
C
MF
GFP
YAPS94A
YAP-TAZ
actin
D
Fusion+GFP
Fusion+YAP(S94A)
E
Trp53−/−KrasG12D/+ Organoids
GFP
YAPS94A
G
DMSO
Defactinib
PF-573228
mTOR
p-mTOR (S2448)
GSKβ
pAKT S473
Total AKT
β-Catenin
S6
β-actin
F
IHC: β-catenin
Mist1-Cre
Fusion
H
Fold Gene Expression (Normalized to Rpl27)
1.5
1.0
0.5
0.0
CTGF
CYR61
MYC
ANKRD1
DMSO
Defactinib
PF-573228

Supplementary Figure 4. FAK inhibition reversed the abnormal morphologies of CLDN18-ARHGAP26.

A, Immunoblotting for the organoids with annotated genotype with *Trp53* knockout. (representative image from 3 independent experiments). **B,** Immunoblotting for the *CLDN18-ARHGAP26* with *Trp53* knockout organoids treated with DMSO, PF-573228 (2 μM) or Defactinib (2 μM) for 48h (representative image from 3 independent experiments). **C,** Immunoblotting for the *CLDN18-ARHGAP26* organoids engineered with GFP or YAP-S94A (n=3 independent experiments). **D**, Representative images of phase contrast of CLDN18-ARHGAP26 organoids engineered with GFP or YAP-S94A. Scale bar = 100 μm. **E**, Representative images of phase contrast of *Trp53*$^{-/-}$*Kras*$^{G12D/+}$ organoids engineered with GFP or YAP-S94A. Scale bar = 100 μm. **F,** Representative images of β-catenin staining for the organoids with annotated genotype. Scale bar = 100 μm. **G,** Immunoblotting for different cancer pathways upon FAK inhibition in *CLDN18-ARHGAP26* organoids (n=3 independent experiments). **H,** Quantitative real time PCR for YAP target genes upon FAK inhibition in *CLDN18-ARHGAP26* organoids (n=3).

Figure S5

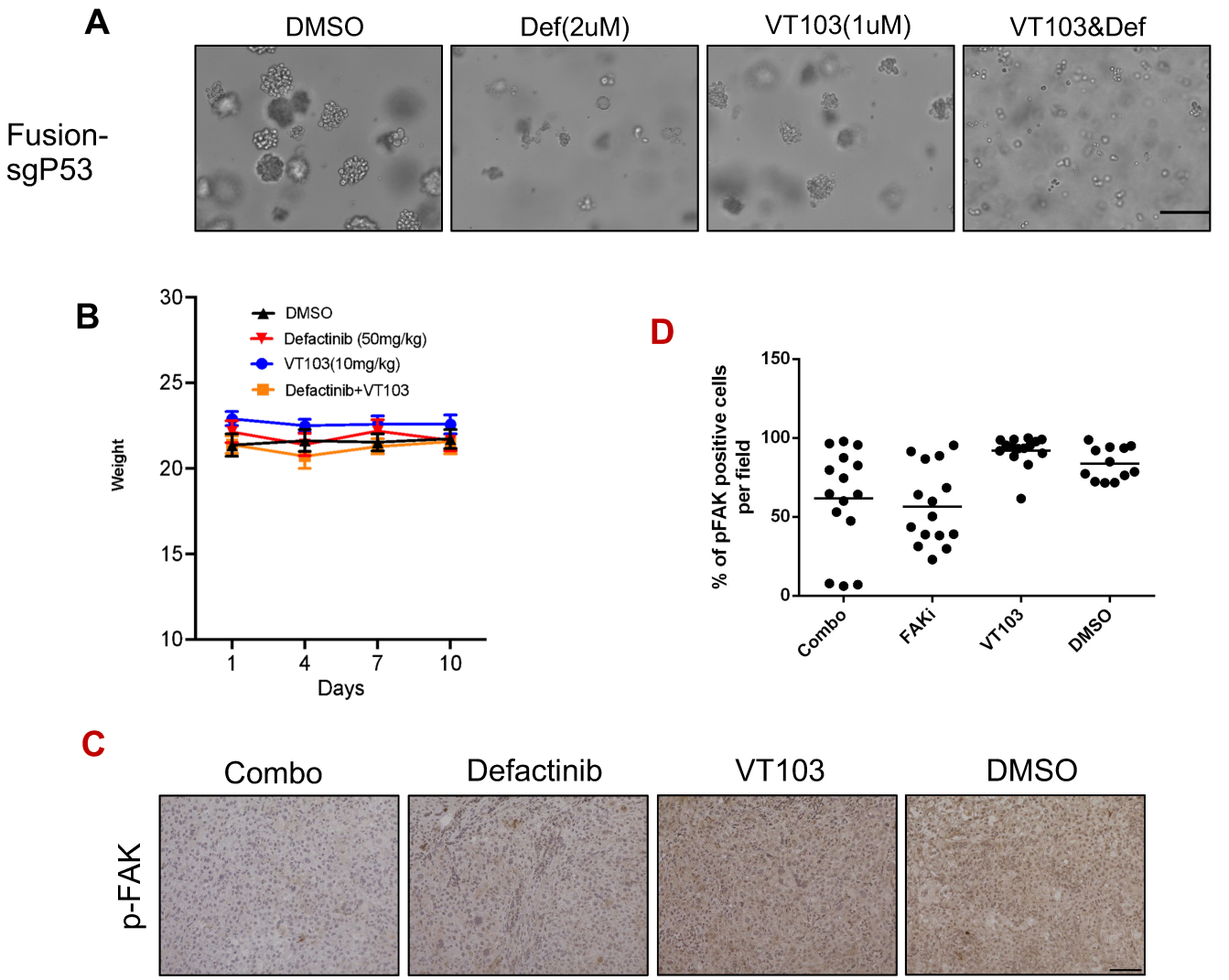

Supplementary Figure 5. Synergistic effect of FAK and TEAD inhibition

A, Representative images of phase contrast of *CLDN18-ARHGAP26* with *Trp53* knockout organoids treated with DMSO control, TEAD inhibitor VT103 (2 μM), Defactinib (1 μM) or the combination for 48h. Scale bar = 100 μm. **B,** Weigh loss curve for *CLDN18-ARHGAP26* with *Trp53* knockout organoids xenograft tumors (n=8-10) treated with vehicle control, defactinib (50 mg/kg, QD), VT103 (10 mg/kg, QD) or the combination. . **C,** Representative p-FAK IHC of xenografts treated with Defactinib, VT103, Combo or DMSO. Scale bar = 100 μm . **D**, IHC quantification for pFAK staining in FAKi (Defactinib), VT103, Combo or DMSO xenograft samples (n=4-5).